THE EFFECT OF RADIATION ON SAW RESONATORS

THE EFFECT OF RADIATION ON SAW RESONATORS

By
Adib Ternawly, B.Eng.
McMaster University
Hamilton, ON

A Thesis

Submitted to the School of Graduate Studies in Partial Fulfillment of the Requirements

for the Degree of Masters of Applied Science

McMaster University

MASTER OF APPLIED SCIENCE (2007) McMaster University

(Electrical and Computer Engineering) Hamilton, Ontario

TITLE: Effect of Radiation on SAW Resonators

AUTHOR: Adib Ternawly, B.Eng. (McMaster University)

SUPERVISOR: Dr. Peter Smith, Professor

Department of Electrical and Computer Engineering

Bachelor of Engineering & Management (McMaster University)

M. Eng, Ph. D. (McMaster University)

P. Eng. (Ontario)

NUMBER OF PAGES: xiii, 82

Abstract

SAW devices are known for their ability to withstand severe operating conditions. However, their data sheets generally provide very little information on their susceptibility to external factors other than temperature. In particular, no mention is made of their sensitivity to ionizing and non-ionizing radiation, even though they are being used in applications where such radiation is present. In this thesis, we report on experiments that we have conducted to measure the impact of intense gamma and neutron radiation on quartz SAW resonators.

Packaged commercial 434 MHz quartz SAW resonators (RFM RP1308) were placed at the output of a Colbalt 60 source and exposed to gamma radiation of up to 50 Mrads. Additional devices were positioned in close proximity to the enriched uranium core of the McMaster University Nuclear Reactor and exposed to intense neutron radiation of 4.5×10^{12} neutrons/cm^{2}s for up to 40 seconds. After waiting for a necessary cool-down period, the irradiated SAW resonators were placed in the feedback loop of a custom oscillator to measure the shift in output frequency as a function of radiation exposure.

Small changes in the oscillator frequency of up to 15 ppm for the gamma radiation and of up to 10 ppm for neutron radiation were obtained in the experiments. However, no clear relationships were observed between the amount of radiation exposure and frequency shift in either case.

Acknowledgements

I would like to start by expressing my sincere gratitude to the Almighty, where in His name, the most gracious, the most merciful, all good things start. I will next list a number of people who I am thankful to; and I apologize to those I forgot or could not mention.

I would like to express my sincere gratitude to my supervisor Dr. Peter M. Smith, for giving me the opportunity to pursue my degree and for his continuous support and guidance throughout my work. It has been indeed an honor to have him as a supervisor, where he showed great understanding, patience and encouragement.

Also, I would like to thank Dr. Haddara and Dr. Novog for taking the time to review my thesis and for being in my committee.

I would next like to thank the friends and colleagues in the ECE department at McMaster University who helped me tremendously throughout the two years of the masters program. To mention a number of them, Tarek Sadek, Munir El Desouki, Waleed Shinwari, Mohammad Haj-Abed, Ali Abu-El-Magd, Ashraf Attala, Moussa Kfouri, Hamed Jafari, Dariusz Palubiak, Ahmed Fakhr, and Kareem Shoukri.

Special thanks to Cheryl Gies who always gave me her time and helped me resolve my problems at McMaster. I would like to thank Mr. Mike Butler, the McMaster Nuclear Reactor manager of reactor operations, and Mr. Robert Pasuta for helping me with my experiments at the reactor. I would also like to thank Terry Greenlay and Cosmin Coroiu for their help with the facilities and components needed for my research.

Next, I would like to thank RF Monolithics for supplying the SAW resonators used in the experiments.

Finally, I would like to express my deepest acknowledgements to my dear family. Mr. Shamel Ternawly, Mrs. Maha Intabi, Mrs. Heba Ternawly, and Mr. Ismail Ternawly have been immensely supportive throughout my career life and a major factor to my success.

List of Abbreviations

SAW	Surface Acoustic Wave
TID	Total Ionizing Dose
MOS	Metal-Oxide Semiconductor
SEE	Single Event Effects
NASA	National Aeronautics and Space Administration
Q	Quality Factor
AW	Acoustic Wave
IDT	Interdigital Transducer
RF	Radio Frequency
SH SAW	Shear Horizontal Surface Acoustic Wave
SH APM	Shear Horizontal Acoustic Plate Mode
TSM	Thickness Shear Mode
VOC	Volatile Organic Compound
ppb	Parts pre billion
ppm	Parts per million
S-FIL	Step and flash imprint lithography
LN	Lithium Niobate
LT	Lithium Tantalite
PZT	Lead Zirconate Titanate
PMN-PT	Single crystal Pervskites
PVDF	Polyvinylidene Fluoride
LGS	Langasite
PMMA	Polymethacrylate
amu	Atomic mass unit
MNR	McMaster Nuclear Reactor
NRB	Nuclear Research Building

List of Symbols

f_0	Oscillation frequency
v	Wave Velocity
λ	Wavelength
K^2	Piezoelectric coupling factor
Δv	Change in velocity
Δf	Change in frequency
v_R	Rayleigh wave velocity
σ_{sh}	Surface conductivity
Cs	Static Capacitance per unit length
h	Planck's constant
c	Speed of light
E	Energy
Z	Atomic number
A	Atomic mass
X	Parent nucleus
Y	Daughter Nucleus
α	Alpha particle - Helium ion
β^-	Betal particle – electron from nucleus
$\widetilde{\nu}$	antineutrino
β^+	Positron
γ	Gamma-ray
n	Neutron density
$n(E)$	number of neutrons per unit volume
T	Temperature
k	Boltzmann constant
m	Mass
$\phi(E)$	Energy-dependent thermal neutron flux

ϕ_T	Thermal flux
F	Collision density
I	Intensity of the monoenergetic neutrons
N	Density of the material
σ_t	Macroscopic cross-section
$\Sigma_a(E)$	Macroscopic absorption cross-section
λ	Radioactive decay constant
$A(t)$	Activitiy
ρ	Physical density
N_A	Avogadro's number
T	Mean lifetime
$T_{1/2}$	Half Life
ΔF_{avg}	Frequency shift in ppm
Φ	Total accumulated dose
f_c	Centre frequency
R_M	Motional resistance
L_M	Motional Inductance
C_M	Motional capacitance
C_0	Shunt static capacitance
ω	Angular frequency
L	Acoustic path length
ϕ_e	Phase change

List of Figures

List of Tables

Table of Contents

Chapter 1

Introduction

1.1 Motivation

Surface Acoustic Wave (SAW) devices have been extensively used in various fields, ranging from TV and radar system components, such as filters, to array of sensors in an electronic nose. Their superior properties compared to other devices, particularly their stability when utilized in harsh environments, raises the question of whether they can withstand, or be used reliably under, nuclear radiation.

Electronic devices, especially the ones used in the signal processing and telecommunication systems, are sometimes subjected to a radiation environment. As such, many of these devices made of semiconductor technologies experience drastic failures when the radiation dose reaches a critical level. Whether for their utilization in space shuttles and satellites, in military applications, or in power and research reactors, SAW resonators' performance should be tested under various types of radiation in order to identify their suitability in such environments.

1.2 Research Goals

A major challenge in microelectronic applications is finding circuits and devices that can operate efficiently in radiation environments. Numerous devices and materials have been tested under the various types of nuclear irradiation; some were proven to be radiation hard (immune to radiation) and others failed at small accumulated doses.

Radiation effects on electronics are divided into 3 categories that depend on the type of effect, and are presented in Table 1.1 [1]. Total ionizing dose (TID) is a type of effect where trapped charges are created in the silicon dioxide gate insulator of a MOS transistor. Displacement damage is another type of effect where hadrons bombarding the silicon lattice of active devices, displaces their atoms, which affects their functionality. The third type, the single event effects (SEE), is not caused after a certain accumulation of radiation dose, whereas, it is related to single interactions in the silicon substrate. In this case, highly energetic ions such as cosmic rays can penetrate the structure of the space craft and reach the electronic components, where one particle can cause any of the listed (in Table 1.1) single effect events.

Table 1.1: Different Types of Radiation Effects on Electronic Components, reproduced [1].

Radiation Environment	Typical Effects
Total ionizing dose	• Threshold shifts in CMOS transistors, leading to failure of logic gates • CMOS filed-oxide charge trapping, loss of isolation, excessive power-supply currents • Power transistor threshold shifts, loss of on/off control • Gain degradation in bipolar-junction transistors
Displacement damage	• Displacement damage effects • Gain degradation in bipolar-junction transistors • Severe degradation of charge-coupled devices, dynamic memory performance • Damage to photodetectors
Single-event effect	• Single heavy ion causes ionization "track" • Temporary logic scramble • Single bit errors in static memories • Localized latchup in CMOS integrated circuits • Gate rapture of power transistors • Temporary upset of analog devices such as amplifiers • Burnout of diodes, transistors • Discharge of capacitors

In order to ensure radiation hardness qualification of electronic components, a set of tests need to be performed. The tests include total dose using an X-ray source (for unpackaged chips) or Cobalt 60 gamma sources, displacement damage using neutrons from a nuclear reactor, and single event tests using high energy proton beams and/or ion beams [1].

According to studies made by NASA, the yearly exposure of radiation dose in space, at geostationary orbits, depending on the aluminium shielding is displayed in Figure 1.1 [2]. The gamma and neutron irradiation tests that were conducted in this thesis were assured to encompass the typical total doses that SAW devices would absorb if used in space satellites or shuttles over an extended number of years. The key contribution of this research study is to further explore the tolerance of high-Q narrow band SAW resonators under rugged environments; to investigate if these compact, millimetre-sized, devices can resist nuclear radiation.

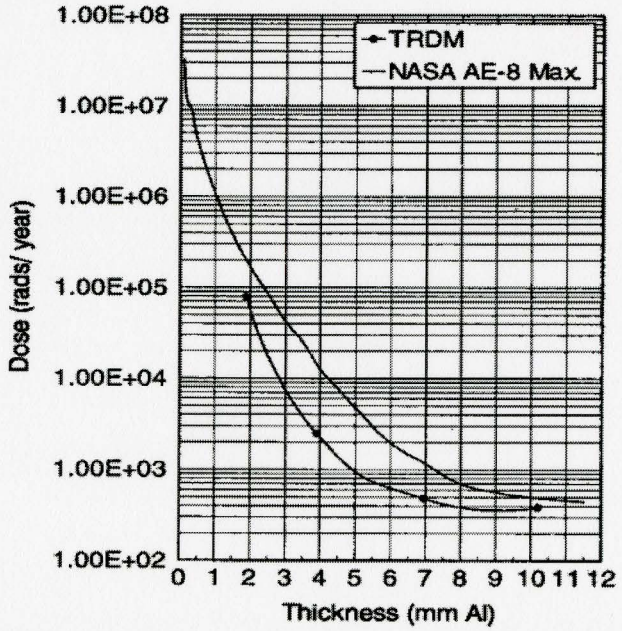

Figure 1.1: Total Radiation Dose per Year as a function of Aluminium Shielding Thickness [2].

1.3 Thesis Organization

An introduction to Acoustic Wave (AW) devices is presented in chapter 2. The chapter starts with the advantages and recent applications of these devices, followed by a background on Surface Acoustic Wave (SAW) devices. The piezoelectric effect and the interdigital transducers (IDTs) are discussed in terms of their interaction that produces the electromechanical coupling that transforms the RF signal into the acoustic wave and vice versa. The types of Acoustic Waves are then reviewed, followed by their sensing mechanisms and parameter sensitivities. Finally a general design technique and fabrication process is described.

Chapter 3 introduces nuclear radiation, starting with the atomic structure and the instability of some nuclei, followed by the different types of emissions to reach stability. The interaction of different radiation types with matter is then described along with the radioactive decay of nuclei and ways of quantifying it.

Combining the knowledge gained from Chapter 2 and 3, Chapter 4 focuses on the effect of nuclear irradiation on SAW devices and other quartz resonators based on previously published papers. A literature review on the topic is presented, where different observations and conclusions based on experimental results are illustrated.

Chapter 5 describes the different experiments conducted on a commercially used high-Q quartz SAW device (RP1308). The experimental setups as well as the procedures for gamma and neutron irradiation are described and their results are displayed, followed by a discussion on the observations and analysis of these results.

Finally, chapter 6 concludes with a summary of this work and a comparison to previous published works. Future work and recommendations are also given in this chapter.

Chapter 2

Surface Acoustic Wave Devices

2.1 Introduction

There has been a growing attention to acoustic wave (AW) devices, in recent years, for several applications. They have been extensively used as filters, resonators, actuators, and sensors. Acoustic wave devices include the surface acoustic wave (SAW), the shear horizontal surface acoustic wave (SH SAW), the shear horizontal acoustic plate mode (SH APM), and the Love wave mode devices [3]. AW devices have been widely used in the telecommunication field and have become an essential part of the cellular phone industry; however as sensors, they are still at an early stage of development. SAW devices have been favoured in the sensing field due to their prominent system of interaction between the acoustic propagation and the measuring parameters. Their exploitation in detecting different physical and chemical parameters has recently increased, ranging from the detection of temperature, pressure, and electric fields to weight percentage in solutions and vapour concentration [4]. The fabrication of these devices is mainly focused on the creation of the Interdigital Transducers (IDT).

2.2 Recent Applications

At first, SAW devices had been widely used in radar systems, TVs, and as RF filters in the mobile and wireless communication industry. As sensors, they are still under development, where more and more applications are discovered and added to this

category. Lately with the vast growing research of the electronic nose (e-nose), SAW sensors have been found essential as chemical or odour sensors. Depositing a chemical layer on the SAW device substrate allows the device to act as a gas sensor. Each type of gas has a corresponding sorbent (or thin-layer deposited on the surface of the device), where the gas molecules bind to when exposed to.

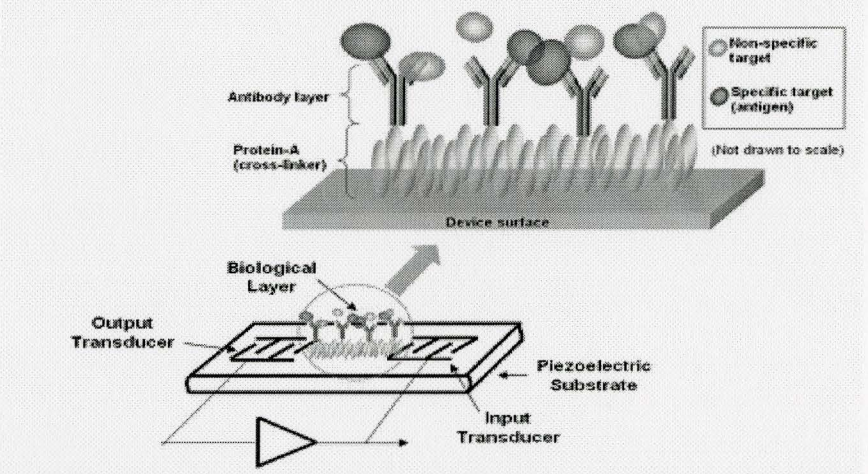

Figure 2.1:Configuration of SAW Sensor for Detection of Low Pressure Explosives [4].

SAW chemical sensors are capable of detecting almost all types of gases. Now they are being used in e-nose devices, where an array of sensors are each set to detect a specific gas or molecule. A recent interesting application of a SAW-based e-nose is the non-invasive detection of lung cancer. There are 11 different volatile organic compounds (VOCs) that, if detected, indicate the presence of lung cancer [5]. By exhaling on the array of sensors (e-nose), different VOCs coming out of the human lung bind to their corresponding sorbents and are detected as previously explained. In addition, a recent paper was published on the detection of low vapour pressure plastic explosives containing nitro groups (such as RDX and TNT) [4]. In this case, the SAW resonator is

coated with an antibody layer that can adsorb the targeted molecules as shown in Figure 2.1.

2.3 Advantages of SAW Devices

- SAW devices are fabricated on highly stable single crystals, making them almost aging-free.
- SAW devices can replace very complex signal processing functions that would require numerous inductors and capacitors, with its simple design of a single piezoelectric crystal, two interdigital transducers (IDTs), and in some cases, a deposited thin-film layer [6].
- Wirelessly, they can be placed on moving or rotating parts and in hazardous environments.
- Where the use of conventional sensors is impossible, dangerous or expensive, they can be used for contact-free measurements under extreme heat or strong radioactive radiation [7].
- They can be mass-produced in compact (millimetre) sizes using microfabrication techniques, where they can be sold for less than $1.00 [6].

2.4 Background on SAW Devices

The development of SAW devices started with the discovery of the piezoelectric nature of quartz. Piezoelectric crystals electrically polarize with the application of an external force, and they exhibit very low internal loss, uniform material density and elastic constants [8]. Along with these properties, their anisotropic (directionally dependent) nature allowed for the wide applications of SAW devices. The different

orientation of the crystal cut leads to the construction of different SAW sensors with different acoustic modes, where each mode is suitable for a specific application.

SAW sensors' main method of detection of physical change in the measurand is through changes to the properties of the acoustic wave traveling on or within its substrate. Acoustic waves propagating on the piezoelectric substrate are generated and detected using metallic interdigital transducers (IDTs), where through a transduction mechanism they convert acoustic (physical) wave signals to electric signals and vice versa. External interference with the surface of the piezoelectric substrate causes perturbations to the properties of the acoustic wave, which are realized by changes in the converted electric signal.

As shown in Figure 2.2, when an ac voltage is applied to the transmitting IDT, an electric field is created between neighbouring fingers, resulting in a strain on the piezoelectric substrate that alternates with the field. The strain travels from the transmitting IDT to the receiving IDT in the form of an acoustic wave. The wave is then detected and transformed into an electric signal with a frequency f_0 given by

$$f_0 = \frac{v}{\lambda}, \tag{1}$$

where v is the velocity of the acoustic wave propagating on the surface of the piezoelectric substrate, and λ denotes the wavelength of the wave. The wavelength is predetermined by the spacing between adjacent electrodes (fingers) and the velocity depends on the type of piezoelectric substrate used.

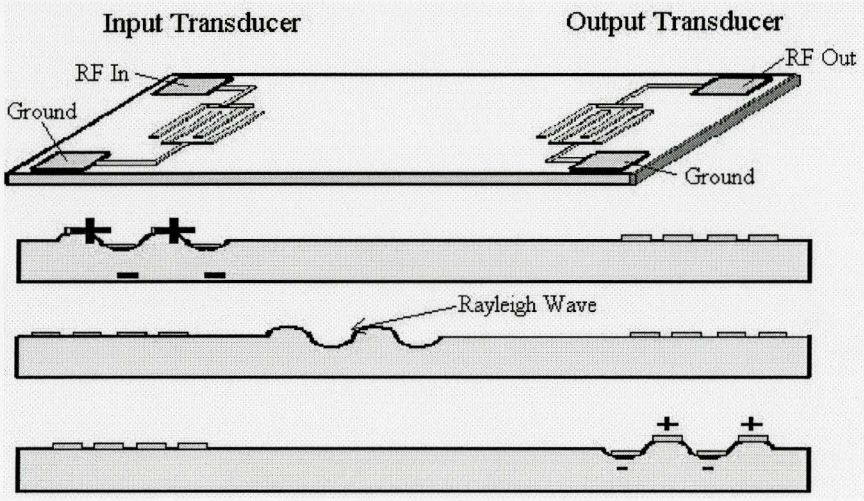

Figure 2.2: SAW device [8]

The sensing mechanism of the SAW sensor depends solely on the change in the velocity of the acoustic wave traveling on or within the piezoelectric substrate between the IDTs [8]. When the velocity of the acoustic wave is changed, the time it takes to receive the wave at the other IDT is altered (lag or lead), which leads to a phase shift in the electric signal. The phase change can be measured using a calibrated system, where a graphical and numerical display of the data is provided, or can be realized by measuring a corresponding frequency shift in the case of the sensor being a SAW resonator and part of an oscillator circuit.

2.5 The Piezoelectric Effect

When a force (tensile or compressive stress) is applied to opposite sides of a piezoelectric crystal, a deformation of the crystal lattice occurs. This leads to a separation of the centers of opposite charges, which creates dipole moments of molecules [9]. As illustrated in Figure 2.3, an electric charge then appears on the surface (electrodes) opposing the net charges on the piezoelectric material [8]. Removing the

force from the material results in current flow from one electrode to another, until a zero potential difference between the electrodes is reached. Furthermore, a sinusoidal voltage will appear across the electrodes when a sinusoidal force (stress) is applied to the material. Therefore a conversion of mechanical to electrical energy occurs in a SAW device at the interface between metal electrodes and a piezoelectric material. This process is completely reversible, meaning that the crystal deforms as voltage is applied across the electrodes. The degree of deformation is proportional to the voltage applied, which leads to the transformation of electrical energy to mechanical energy.

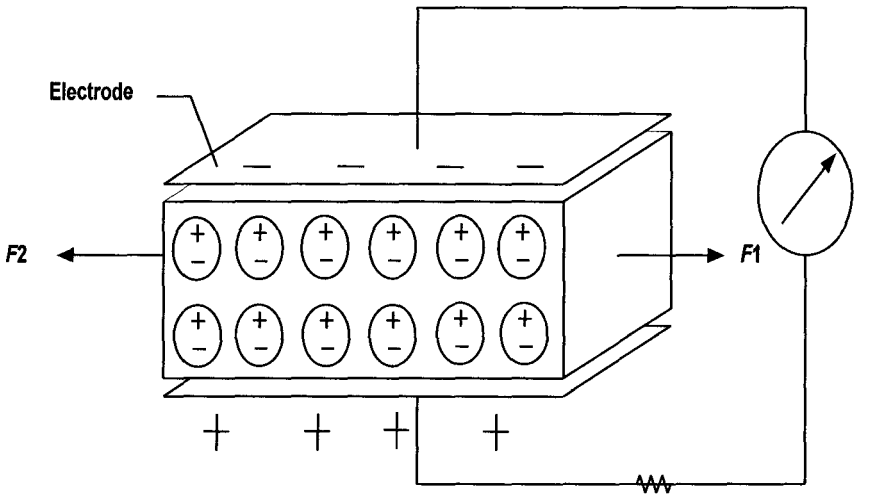

Figure 2.3: Transformation of mechanical energy to electrical energy in a piezoelectric material [8].

The piezoelectric effect happens when the crystals in a material have nonsymmetrical centers. The crystals' crystallographic structures can predict the piezoelectric properties, where depending on the properties, they are used in various suitable applications [8,9]. In fact, they can be used for a wide range of frequencies depending on the crystal angle of cut (anisotropic nature), which also determines the angle and type of wave propagation on or within the substrate.

Aside from the crystallographic structure and the angle cut of the crystals, the piezoelectric coupling factor K^2 of the substrate used is a very significant parameter. K^2 is also known as the electromechanical coupling coefficient and it measures the strength of the piezoelectric coupling. This parameter determines the maximum attainable bandwidth of the AW, where for a given insertion loss, the maximum bandwidth is larger for higher K^2 values [10].

2.6 Interdigital Transducers

The Interdigital Transducer (IDT) is a fundamental part of SAW devices. The actual transformation of energy occurs at the IDT, where the acoustic wave is generated and detected. Figure 2.4 shows the structure of the IDT. The IDT is composed of two comb-shaped metal electrodes fabricated on a piezoelectric substrate. As mentioned earlier, elastic waves are created as a result of induced strains in the piezoelectric material by an applied voltage. The acoustic wave created travels with a velocity v in both directions, normal to the electrodes, along the piezoelectric substrate. The IDT has to be fabricated in a way where the distance d between consecutive electrodes is equal to half the AW wavelength λ to ensure constructive interference of the generated waves [8].

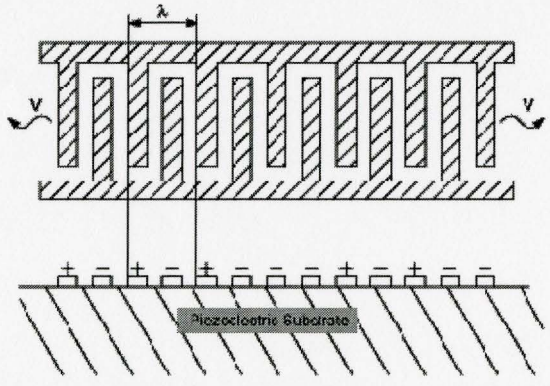

Figure 2.4: General Structure of an Interdigital Transducer (IDT) [11].

The electrodes of the IDT are usually made of either an aluminium layer or a layer of chromium attached to a gold layer. The chromium is used as an adhesion between the gold layer and the quartz, but is not required with aluminium, since aluminium is highly adhesive to quartz. The mass of the IDTs' metal electrodes dampens the acoustic wave; hence lighter metals will reduce this damping effect, and this is why Aluminium is typically preferable to gold for IDT metallisation. To achieve minimum damping of the acoustic wave, the metal electrodes should be as light as possible, but that should not significantly influence their electrical resistance. Accordingly, the thickness *h* is usually in the range of 500 to 2000 Å to provide a good electrical contact and low resistance, while maintaining low damping of acoustic wave [6].

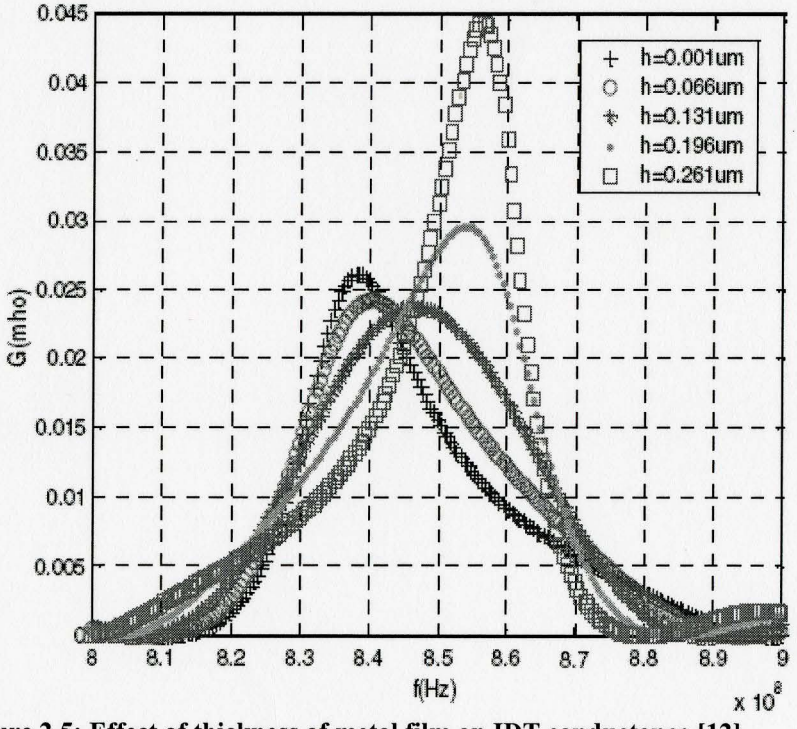

Figure 2.5: Effect of thickness of metal film on IDT conductance [12].

According to literature, varying the thickness of the electrodes has secondary effects; however, no expressions have been developed to model these effects. Figure 2.5 shows the effect of varying the thickness on the IDT conductance and the resonance frequency [12]. As presented in the figure, the relationship between the thickness of the metal and the conductance is not clear; however, it is apparent that as the thickness is increased, there is an increase in the resonance frequency.

2.7 Types of Acoustic Waves

The type of acoustic wave depends on the properties of the piezoelectric material, the crystal cut, and the structure of the electrodes (IDT). The main types of acoustic wave sensors are Rayleigh SAW, shear horizontal SAW (SH-SAW), love wave, acoustic plate mode (APM), and flexural wave (FPW).

2.7.1 Rayleigh Surface Acoustic Waves

The Rayleigh wave, discovered by Lord Rayleigh [13], has been referred to as the SAW until recently. Rayleigh SAWs have been known for their high sensitivity of detection in gaseous environments. The wave travels along the piezoelectric substrate as a result of the physical disturbance created by the IDT, and it has a surface-normal component and a surface-parallel component that both travel in the same direction. The movement of the particles that characterizes the wave follows an elliptical motion that lays on the same plane as its wave components, as shown in Figure 2.6. Rayleigh waves penetrate into the surface at depths on order of magnitude of their wavelength [14]. Along with the acoustic wave, there exists an EM wave associated with it and that

propagates in the same direction. The velocity of the wave, as mentioned before, depends on the piezoelectric crystal cut and substrate material.

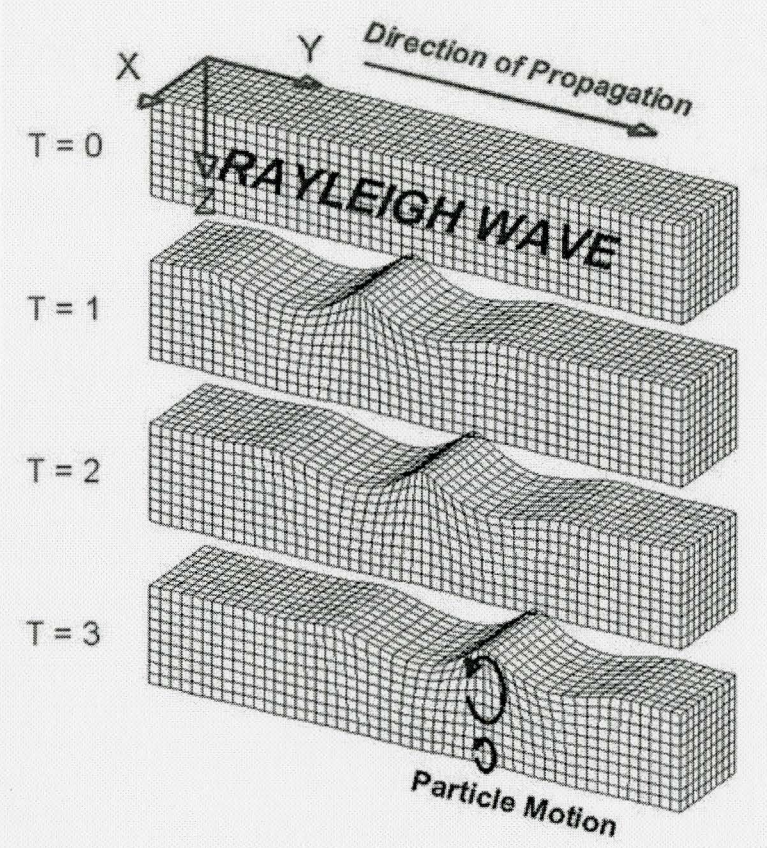

Figure 2.6: Rayleigh-wave propagation through an elastic material. The disturbance that is propagated is an elliptical motion which consists of both vertical (shear; perpendicular to the direction of propagation but in the plane of the raypath) and horizontal (compression; in the direction of propagation) particle motion. The material returns to its original shape after the wave has passed [6].

A typical SAW device consists of two IDTs on a quartz substrate, where one IDT is for generating the acoustic wave and the other is for detecting it. The receiving IDT is usually connected to an amplifier, in which the received wave is amplified after being converted to an electrical signal then analyzed using a sampling device [8]. A sampling device could be a spectrum analyzer, where the power of the signal (in dBm) is plotted against a range of frequencies, or could be a network analyzer that displays the phase

properties of the signal. A change in the properties of the acoustic wave due to external factors, such as change in pressure, temperature, or adsorption of foreign atoms, is measured by changes in the properties of the electric signal. The relation between changes in the wave velocity to changes in the signal frequency is shown by

$$\frac{\Delta v}{v_R} = \frac{\Delta f}{f_0}, \tag{3}$$

where Δv is the change in the acoustic wave velocity, v_R is the Rayleigh wave velocity, Δf is the change in frequency, and f_0 is the designed oscillation frequency of the wave.

2.7.2 Shear Horizontal Acoustic Waves

As mentioned earlier, different crystal cuts result in different acoustic wave modes. The piezoelectric crystal is cut in a way, typically a 37^0 rotation Y-X cut for a quartz material (as presented in Table 2.1), where a SH surface wave is created to travel horizontal to the surface of the device as shown in Figure 2.7. As opposed to SAW devices, SH-SAW devices are favoured for biosensing in an aqueous environment, since they do not radiate acoustic energy into the liquid media which would result in the wave's rapid attenuation [15]. SH-SAW is known for its sensitivity to mass-loading, viscosity, conductivity, and permittivity of liquid [8]. Although they are similar to the structure of SAWs, the wave tends to propagate deeper in the substrate and are sometimes referred to as surface skimming bulk waves.

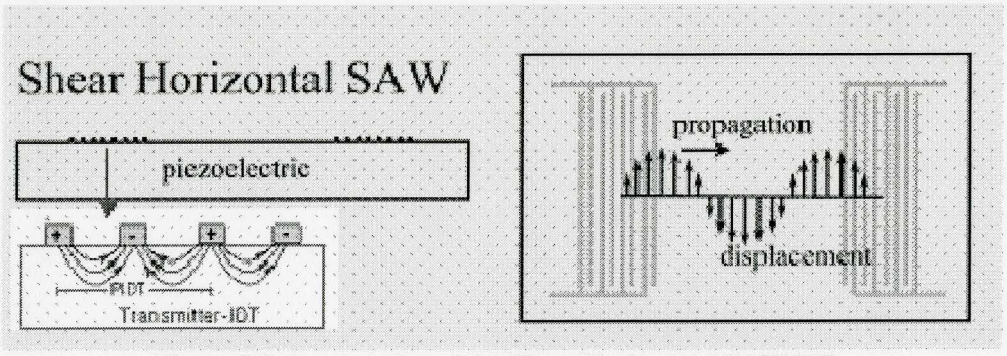

Figure 2.7: Propagation of the Shear Horizonatal SAW [16].

Table 2.1: Piezoelectric material properties at RT of common SAW sensor substrates (LN: lithium niobate, LT: lithium tatalate, and LGS Langasite = La3Ga5SiO14), reproduced [17].

Material	Orientation	Wave type	v_{ph} (m/s)	K^2 (%)	TCD (ppm/^{0}C)	Tmax (^{0}C)
Quartz	ST-X	Generalized Rayleigh	3158	0.1	0	550
	37^{0}rot Y-X	SH	5094	≈ 0.1	0	550
LN	Y-Z	Rayleigh	3488	4.1	94	(600)
	41^{0}rot Y-X	Leaky SH	4750	15.8	69	(600)
LT	36^{0}rot Y-X	Leaky SH	4220	≈ 6.6	30	<610
LGS	Y-X	Rayleigh	≈ 2330	≈ 0.37	≈ 28	>1000

Shear Horizontal Acoustic Plate Mode (SH-APM) devices also have a similar design to Rayleigh SAW devices, but with a thinner substrate. The SH waves generated by the IDTs of these devices, propagate at angles from the surface into the bulk and get reflected between the surfaces of the substrate (as shown in Figure 2.8) until they reach the receiving IDT [3]. In this case, the thickness of the substrate and the spacing between the IDT fingers are what determine the frequency of the acoustic wave. The propagation of the acoustic wave in the SH-APM device allows for the separation of the liquid sensing part from the IDTs, avoiding chemical reaction problems. Since the wave is reflected off the sensing surface, any changes in the parameters of the measurand (sensed

liquid) will result in a change of the SH wave properties. As with the SAW sensor, a change in the wave properties is detected by a change in the properties of the electric signal. Therefore a shift in phase will occur if the mass, viscosity or density of the liquid is altered.

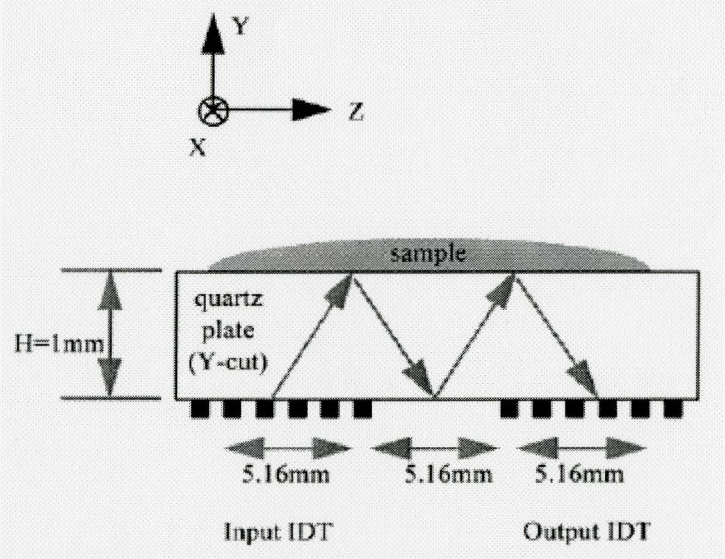

Figure 2.8: Propagation of the Shear wave in a SH-APM device [3].

2.7.3 Love Surface Acoustic Waves

Love waves are considered SAWs that propagate in a waveguide made of a thin material and deposited on a substrate made of another material [18]. The substrate has different acoustic properties and is of infinite thickness when compared to the deposited thin layer (waveguide). Figure 2.9 describes a general structure of a Love SAW and illustrates the propagation of the Love AW [10,14]. A love wave, propagating in the x-direction, brings shear stresses (mechanical displacement) only in the y-direction. The acoustic waves transmitted by SH-APM devices, on the other hand, get reflected from one surface to another within the substrate (traveling through the crystal bulk) and thus are limited by the diffraction of the signal in the bulk, and background interference when

reflected off the bottom surface [8]. The role of the top layer of the Love SAW, typically SiO_2, is to guide the wave in traveling in the top layer, which in turn prevents the device from falling into the disadvantages associated with the SH wave-based device.

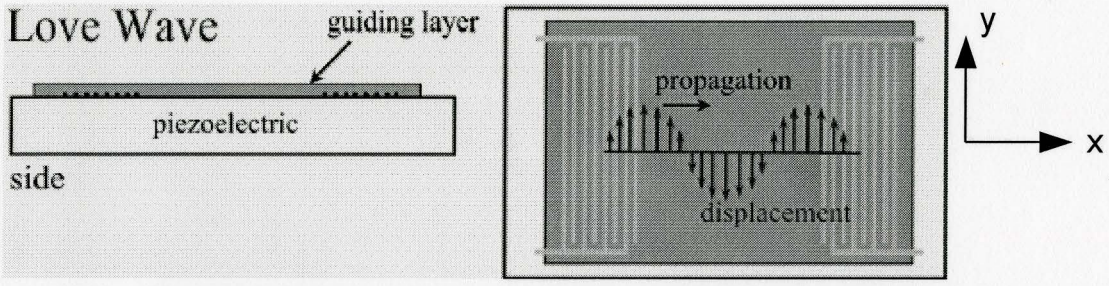

Figure 2.9: Piezoelectric device structure and type of propagation [14].

A necessary condition for obtaining the Love wave is that the shear wave velocity in the first (guiding) layer must be lower than that of the second (substrate) layer [19]. The principle behind the generation of Love waves is very similar to the one used for SH-SAWs except for the waveguide layer that is deposited over the IDTs. As mentioned earlier, this layer ensures a horizontal propagation of the wave between it and the piezoelectric (second) layer, where the IDTs are placed. Just like SAWs and SH-SAWs, the wavelength of the acoustic wave depends on the IDT spacing between the fingers, and the shear wave velocity relies on the propagating material (guiding layer).

Love wave sensors are typically employed for liquid sensing applications due to their mechanical robustness as well as their high sensitivity [20]. They are sensitive to the permittivity and conductivity of the detected liquid. The advantage Love SAW devices have over SH-SAW devices is that the loading of the measurand is on the same surface of the sensing area [8]. Their loading is directly over the IDT, but separated by a

very thin layer. An optimum thickness for the SiO_2 waveguide has been proven to be 0.18 times the Love wavelength [20].

2.8 Sensing Mechanism and Parameter Sensitivity

Since the piezoelectric material is an integral part of acoustic wave devices, the parameters that are calculated from the sensors' results must involve either mechanical or electrical perturbation. Therefore the values of certain parameters, such as chemical concentrations detected by chemical sensors, would need to be transformed into mechanical or electrical perturbations that will disturb the properties of the acoustic wave [3].

The acoustic velocity is mainly perturbed by either one or a combination of the following: mass, electrical, or environmental parameter properties. Due to the direct relation between the acoustic velocity and phase, the phase of the electric signal is also perturbed by the same parameter properties. SAW devices are commonly used to sense the following parameters: temperature, pressure, mass loading, viscoelasticity, and conductivity [21].

2.8.1 Temperature

Temperature is considered the easiest parameter to be sensed because temperature has an effect on any chemical or physical structure. In AW sensors, variation in temperature creates dimensional, mechanical and electrical property changes. This leads to a shift in the acoustic velocity resulting from a change in material properties in SAW

sensors, and a change in material properties and boundary conditions in other sensors like SH-APM [3].

The temperature sensitivity of SAW devices can be effectively used for other interesting applications. Measuring the dew-point of humidity is one example. It requires decreasing the temperature and monitoring the change in frequency of the converted electric signal (in an oscillator form). As the temperature reaches the point where condensation occurs, water vapour appears on the Rayleigh wave propagation path, which leads to amplitude attenuation and change in the velocity of the wave due to mass loading [3]. As depicted in Figure 2.10, the frequency tends to vary linearly with a change in temperature, until the temperature drops below the dew-point [22]. Temperatures below this point result in a rapid decrease in the acoustic wave velocity, which will be realized as a sudden drop in the centre frequency of the resonators in an oscillator circuit.

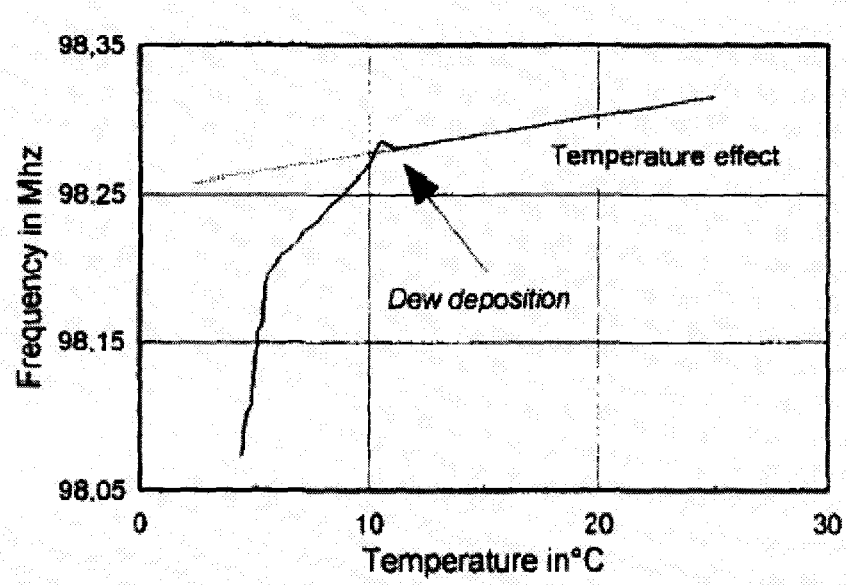

Figure 2.10: Effect of Due Deposition on the Frequency versus Temperature Curve. [22]

2.8.2 Pressure

SAW sensors can detect change in pressure since pressure causes mechanical loading to the device. The pressure induces strain on the substrate, which affects the properties of the AW and results in a phase change to its oscillation frequency. A very useful application for pressure SAW sensors is the continuous measurement of a vehicle's tire pressure. Figure 2.11 illustrates different methods of measuring an applied pressure to the sensor, but they are both based on the bending of the device [23].

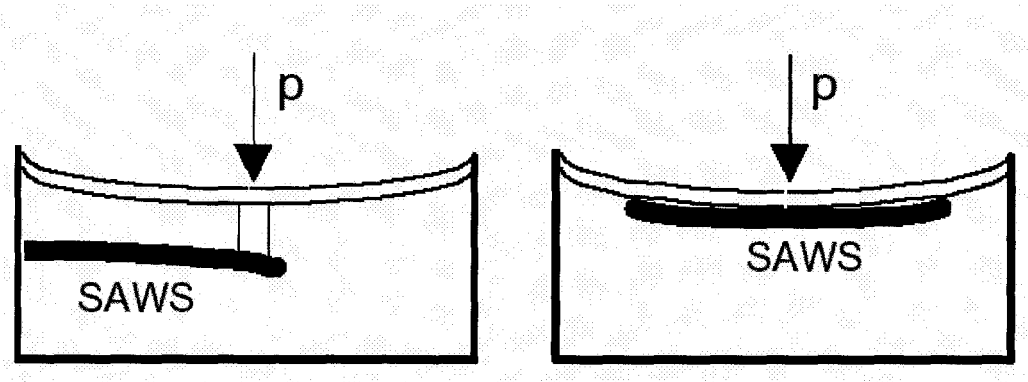

Figure 2.11: SAW Device Pressure Measurement through Membrane Bending [23].

2.8.3 Mass Loading

Due to its various applications, mass loading is an interesting sensitivity parameter to utilize in the SAW sensor field. Film thickness monitoring, gas and liquid media chemical and biochemical sensing are common applications of this type of parameter sensing. Biochemical SAW sensors in particular are extensively used in measuring gas and liquid properties, and they are known for their remarkable sensitivity, ruggedness and stability. This is achieved by coating the SAW sensor substrate with a biochemical thin film layer, where the coating varies with the type of measurand being

sensed [3]. The interaction between the deposited thin film and the desired entity to be sensed causes a change in the velocity of the AW.

The device's geometry and center frequency affects the mass sensitivities of acoustic devices. For SAW and SH-SAW devices, increasing the center frequency (and decreasing the substrate thickness for SH-APM) leads to an increase in the mass sensitivity [3].

The mass loading sensitivity parameter requires certain attention to the analysis of the sensing mechanism, since there may be significant sensitivity interference from other environmental parameters like temperature, pressure and viscosity. Some researchers have been focusing on this issue, especially for AW gas sensors and biosensors [8].

2.8.4 Viscoelasticity

Viscoelasticity could be an influential factor in the sensing of a desired parameter. A study of the effect of the viscosity on the measurand sensitivity is vital for the sensing applications in liquids. In general, SH-APM and SH-SAW are the most suitable devices for sensing viscosity, especially SH-APM, since its liquid sensing region is separate from the transduction area.

The measurement of the viscosity of a liquid is realized by measuring the attenuation of a shear acoustic wave that is reflected off the liquid-substrate surface interface [24]. Water-glycerin mixtures have been used to demonstrate the attenuation of the AW at different viscosity levels and at a given temperature. Figure 2.12 is a plot of the insertion loss with different glycerin water mixtures after one reflection off the liquid-quartz interface [3].

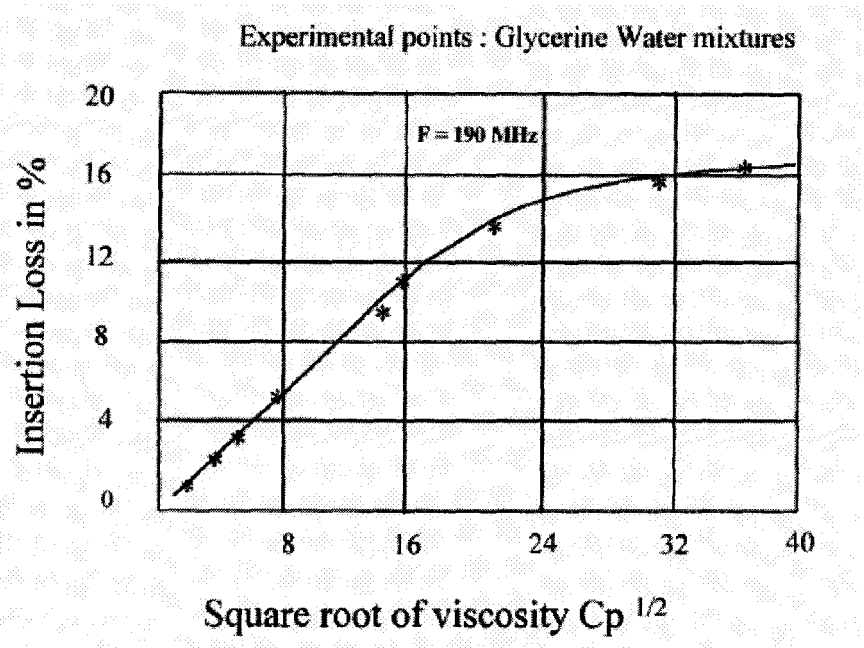

Figure 2.12: Insertion Loss in Percentage of SH-APM device for various viscosities [3].

2.8.5 Conductivity

In gas and liquid medium applications, conductivity plays a major role as a sensitivity parameter in acoustic sensors. The sensing mechanism for this parameter is through electrical perturbation (acoustoelectric effect) of the AW. The electric perturbation occurs as a result of the acoustoelectric interaction with the liquid or gas [25], where the AW propagating at the surface of the device has an associated electric field that extends into the measurand and interacts with its charge carriers [26].

This mechanism could be clearly explained through a new application of the conductivity sensitivity parameter of a SAW sensor. Depositing a semiconducting oxide thin film on the substrate of a SAW device, allows for the detection of change in oscillation frequency due to variations in film conductivity. The change in frequency of the detected signal can be given by

$$\frac{\Delta f}{f_0} = \frac{K^2}{2 \times \sigma_{sh}^2 / \left(\sigma_{sh}^2 + \sigma_0^2\right)} = \frac{-\Delta v}{v_0}, \tag{5}$$

where K^2 is the piezoelectric coupling constant of the substrate, σ_{sh} is the surface conductivity of the film, and $\sigma_0 = v_0$ x C_s, where C_s is the static capacitance per unit length of the substrate surface [27]. In the case of a SAW-based ozone sensor, the SAW propagates through $LiNbO_3$ coating (over the piezoelectric substrate) and the quasi-static electric field coupled with the SAW interacts with the ions in the film. The velocity of the AW varies with the film conductivity, which then is measured by a change in the oscillation frequency. A representation of the change in frequency due to a change in ozone concentration over time is shown in Figure 2.13 [3]. As the sensor was exposed to 50 ppb ozone concentration, a 100 ppm positive change in frequency occurred, whereas when a 150 ppb ozone concentration was added, a 300 ppm positive change in frequency took place. The air added between each concentration measurement is to restore the sensor to its original form (remove the effect of the previous measurand on the sensing layer), and prepare it for the next measurement.

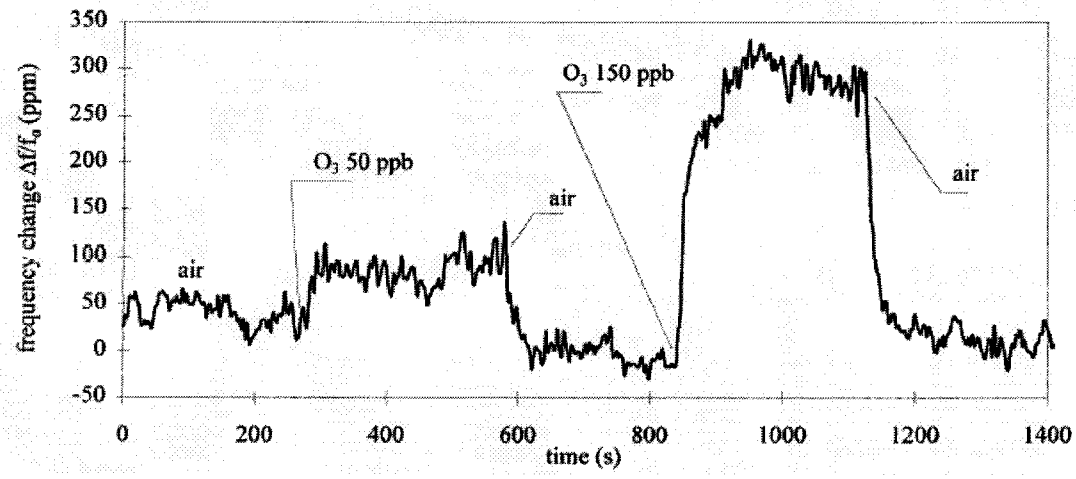

Figure 2.13: The Response of SAW Ozone Sensor to Change in Concentrations at a Given Temperature [27].

2.9 Design Techniques and Fabrication

In designing an acoustic sensor, several issues need to be carefully considered before the implementation of the design. These issues include acoustic wave mode selection and sensitivity, substrate selection, transducer geometry and the thin film material and deposition technique selection (for gas and liquid sensors) [3].

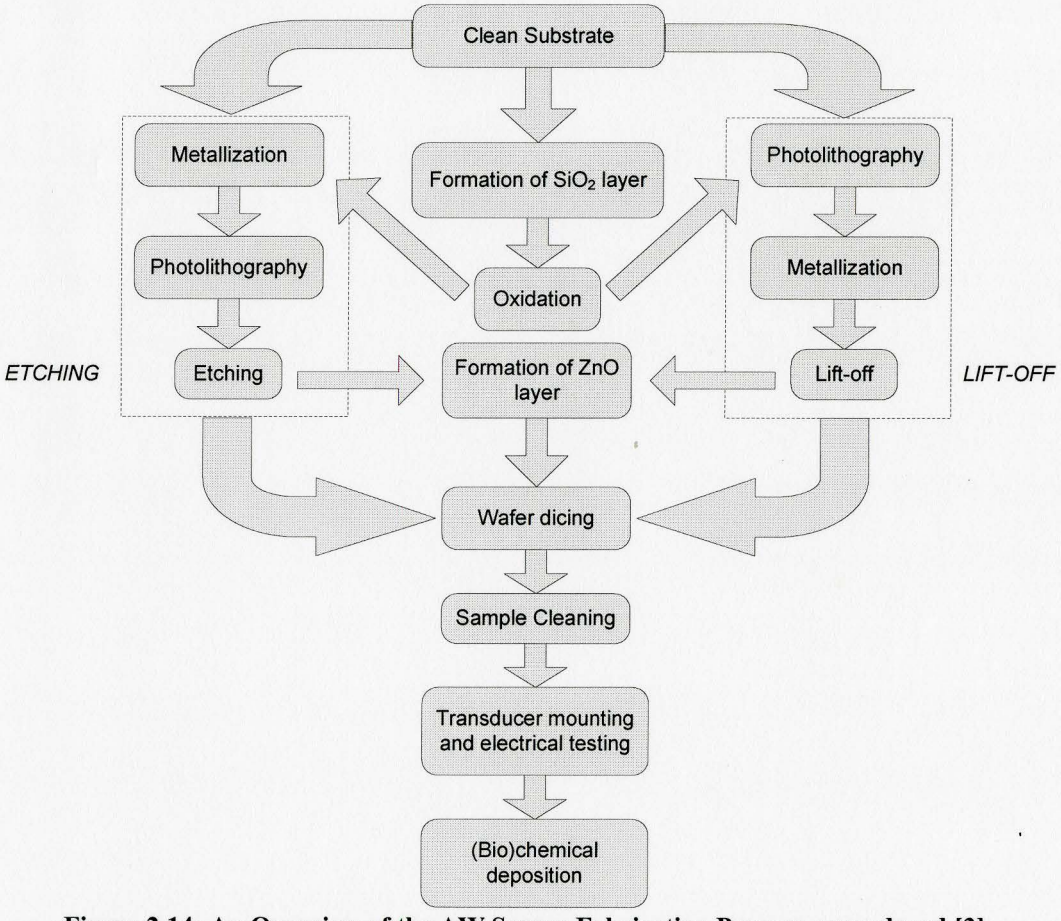

Figure 2.14: An Overview of the AW Sensor Fabrication Process, reproduced [3].

The fabrication process of an AW device depends on the material selected for the substrate. Figure 2.14 summarizes the fabrication steps for a general AW device [3], where etching and lifting off methods of removing unwanted metal parts are commonly

used for the fabrication of the IDTs. The etching procedure includes the utilization of a positive mask in the photolithography step followed by the removal of the unwanted metal. The removal of the undesired metal depends on whether a positive or negative photoresist have been used. The lift-off method, on the other hand, uses a negative mask in the photolithography step to create a photoresist pattern on the structure before the metallization step. The removal of the unwanted metal is easily done due to the discontinuity that appears at the surface of the substrate after the evaporation of the metal.

The choice of material to be used as the device's substrate is characterized by its elastic linearity, low loss or high quality factor, zero temperature coefficients of frequency, and most importantly its piezoelectric property. Quartz has been the most commonly used piezoelectric material for SAW devices due to its extremely high quality factor. Later, lithium niobate (LN) and lithium tantalite (LT) were introduced as a result of the bandwidth limitations of quartz due to its low piezoelectric coupling. Only recently have other materials such as GaAs, ZnO, AlN, SiC, lead zirconate titanate (PZT), single crystal pervskites (PMN-PT), and polyvinylidene fluoride (PVDF) been added to the list of available piezoelectric materials [28]. The demand for piezoelectric materials with higher quality factor, increased bandwidth, better temperature stability, and higher acoustic velocity led to the development of langasite (LGS).

Apart from the selection of the suitable substrate and wave type, the design of the transducer including the number and geometrical form of the electrodes is very important. As has been mentioned earlier, the spacing between the electrodes must equal

half the wavelength of the AW to ensure constructive interference between the waves generated by each electrode. In order to achieve good oscillation frequency stability, there should be a long delay time in the device, which is implemented by creating a long delay line. To ensure an oscillation of only one frequency at any given time, the total length of both IDTs must be more than 90 percent of the center-to-center distance between the two transducers. It is also preferable to limit the number of electrodes in each IDT to 120, and this will only leave 5 percent of the device to be the active acoustic area. Additional electrodes is good for achieving lower insertion loss, but this increases the influence of metal on frequency accuracy, turnover temperature, and triple transit reflections [29].

There are different techniques for fabricating the electrodes of the IDTs in SAW devices. The fabrication of IDT using electron-beam lithography is difficult for non-conductive piezoelectric materials. In this case, imprint lithography would be a useful technique since it is known for its simplicity and lower cost when using a sub-100 nm resolution. However it is predicted that the next generation fabrication technique would be the step and flash imprint lithography (S-FIL) technique.

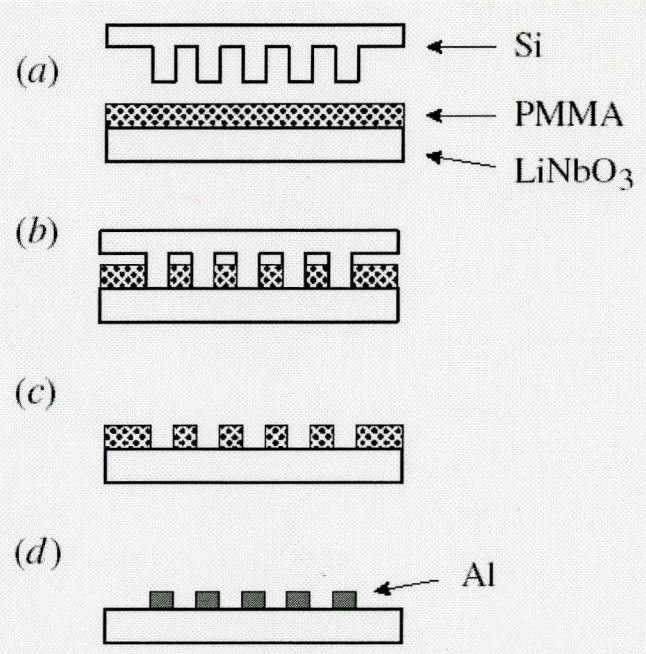

Figure 2.15: Schematic Diagram of the Device Fabrication Procedure using Imprint Lithography. (a)The mould is pressed onto the resist-coated substrate. (b) While the mould is compressed towards the substrae, they are heated to 170^{0}C. (c) The mould is removed after cooling down to RT. (d) Electrode metal structure is created from the resist pattern using the lift-off method [30].

An example of such techniques would be the fabrication of IDTs on a lithium niobate ($LiNbO_3$) substrate using nanoimprint lithography. Figure 2.15 demonstrates the fabrication steps of this technique [30]. $LiNbO_3$ is first cleaned using sulfuric acid (H_2SO_4) solution and O_2 plasma. A 180 nm resist layer of polymethacrylate (PMMA) is deposited over the $LiNbO_3$ layer. A mould made of Si is then compressed onto the resist coated layer, while being heated for 10 min to a temperature of 170^{0}C. Prior to releasing the mould from the substrate, the sample is cooled down until it reaches a temperature point, where below it the PMMA turns into glass. Before the metallization step, oxygen plasma etching is used to ensure that all the PMMA is removed from the bottom of the trenches. The PMMA is then removed using the lift-off technique, and a finger-like metal structure remains over the substrate. The gate metal consists of an Al layer (30

nm) sandwiched between Ti layers (60 nm). They were fabricated to have a width of 170 nm and spacing of 0.6 μm [30].

2.10 Conclusion

Surface Acoustic wave devices have been gaining great attention due to their high sensitivity to numerous parameters in liquid and gas media. The discovery of the piezoelectric effect in certain materials and the development of the IDTs helped in creating the SAW device. In this chapter, the general structure and the mode of operation of the device have been explained, and a number of applications have been discussed along with the demonstration of the different types of SAWs. Depending on the type of SAW selected and the measurand to be sensed, the design of the device would vary. Once the design has been established, the piezoelectric material and geometry of the IDTs is to be determined. This chapter gave a useful background on the device examined for this thesis, which will facilitate the understanding of the experiments conducted and results obtained.

Chapter 3

Introduction to Nuclear Physics

3.1 Stability of the Nucleus

Out of more than 110 chemical elements, 90 elements exist naturally on earth. Most of these elements form stable atoms, which do not change their properties while going through radioactive decay. In addition to very few naturally occurring atoms, all man-made atoms are unstable [31].

Plotting the number of neutrons in stable isotopes as a function of the atomic number, Z, shows that the number of neutrons increases as the number of protons increases. As shown in Figure 3.1, each circle represents at least one stable isotope for a particular element, where additional circles represent other stable or unstable isotopes. From the trend of the circle distribution in the chart, it is apparent that the number of neutrons is almost the same as the number of protons for lighter nuclides. As the atomic number is greater than 20, the number of neutrons starts to increase when compared to protons reaching ratios of about 1.3 and 1.5 for intermediate and heavy nuclides, respectively. The extra neutrons are essential in holding the nucleus together by overcoming the long-range repulsive coulomb forces between the protons. However for nuclides with Z greater than 83, the extra neutrons cause instability to all their isotopes [31].

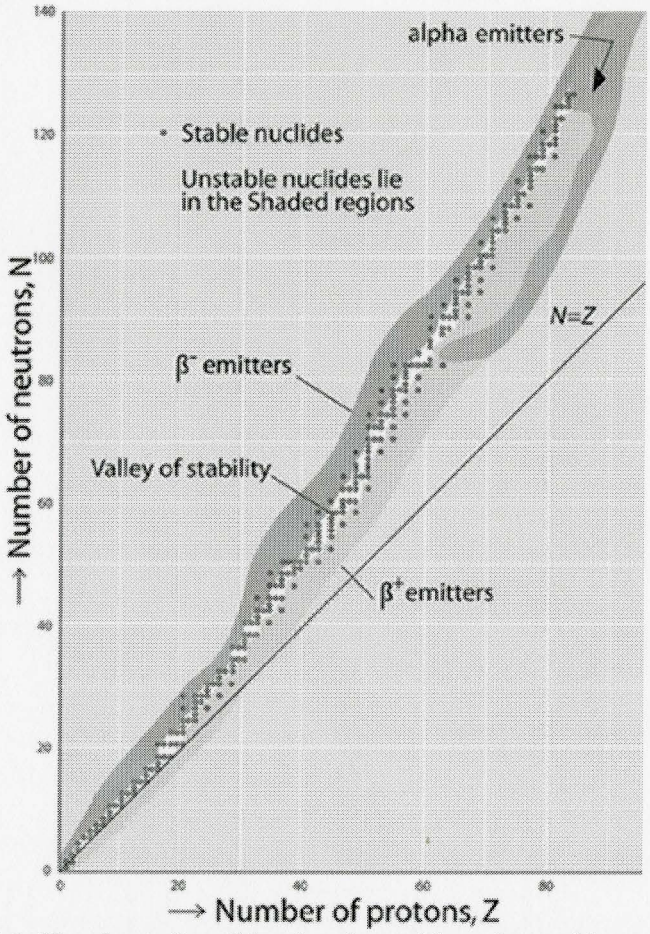

Figure 3.1: The chart of nuclides showing stable and unstable nuclei [33]

As presented in Figure 3.1, there is a valley of stability, where if nuclides lie in this range of neutron-to-proton ratios they are most likely stable. Any stable nuclide has to be in this range of ratios and any nuclide outside this range is unstable; however, it is not necessary that any nuclide in this range is stable. There are two models, namely the liquid drop model and the nuclear shell model that explain some of the conditions of stability of the nuclei, but neither is capable of implicitly describing all the nuclei's characteristics [31]. The liquid model will be used in a later section when describing the fission process that a nucleus may undergo after the absorption of a neutron. The nuclear

shell model is useful in its explanation of nuclei that are unusually stable. There is a set of numbers, named magic numbers, where if the total number of either neutrons or protons pertaining to a nucleus is equal to one of these numbers, then the nucleus must be stable. The magic numbers are as follows: 2, 8, 20, 28, 50, 82, and 126 [32]. Nuclei with magic numbers are useful in some applications, since they are not as prone to neutron absorption as much as other elements' nuclei. They are particularly useful as structural materials in reactors when neutron absorption needs to be avoided [31].

3.2 Radioactivity and Radioactive Decay

Nuclides having an atomic number greater than 83, in addition to several naturally occurring ones with atomic number less than 83, and many artificial radioactive nuclides are unstable [31]. They are radioactive and decay by emitting an alpha or a beta particle to attain a more stable configuration [34]. The new nuclides formed, referred to as daughter nuclides; continue decaying until a stable nuclide with an atomic number of 83 or less is reached. There are three types of radiations that are produced as the unstable nuclides go through the process of disintegration, the alpha particle, beta particle, and gamma photons emissions.

3.2.1 Alpha Emission

An alpha particle is a strongly ionized helium-4 nucleus stripped off of its two orbiting electrons. Generally, the alpha particle is emitted from a heavy nuclide (heavier than lead) as part of its radioactive transformation [32]. This type of transformation can be expressed by the equation,

$$X_Z^A \rightarrow Y_{Z-2}^{A-4} + \alpha . \tag{3.1}$$

The decaying nucleus is referred to as the parent nucleus and is represented by the symbol X in this equation. The nucleus produced as a result of the emission, the daughter nucleus represented by Y, shows that the parent nuclide lost 4 atomic masses (2 neutrons and 2 protons) which is equivalent to the alpha particle.

3.2.2 Beta Emission

Beta particles are fast electrons emitted by radioactive nuclei; however they are electrons of nuclear origin and not of orbiting nature. They have the same mass and charge as any electron, and they travel at speeds close to the speed of light (0.9c– 0.99c) [31]. The conversion of one neutron into a proton in the nucleus is what results in the emission of the beta particle, β^-. This type of decay is common for unstable nuclei with neutrons outnumbering protons, where the neutron-to-proton ratio becomes smaller, resulting in the nucleus to be closer to the stability region (as shown in Figure 3.1).

Along with the beta particle, a subatomic particle, called antineutrino, is produced. This particle; however, has a very small mass and no charge, which makes it hard to define. It is not a significant source of energy, since it travels subtly through matter with slight interaction. As depicted in the equation representing beta emissions,

$$X_Z^A \rightarrow Y_{Z+1}^A + \beta^- + \tilde{\nu} , \tag{3.2}$$

the atomic mass number remains the same. On the other hand, the atomic number is increased by one, making the daughter nuclide move up one position in the periodic table of elements [1,2].

Another type of beta decay, which happens less often, occurs when a proton converts to a neutron followed by an emission of a positron and a neutrino. A positron is similar to an electron, having the same mass but an opposite charge; whereas the neutrino is like an antineutrino with the exact same properties. This decay, referred to as a β^+ decay, takes place when the number of neutrons is less than protons, whereby increasing the number of neutrons by one brings the nucleus closer to the stability line. The following equation describes this type of decay, depicting the unchanged atomic mass number and the decrease in atomic number:

$$X_Z^A \rightarrow Y_{Z-1}^A + \beta^+ + \nu, \tag{3.3}$$

where β^+ symbolizes the positron and $\tilde{\nu}$ resembles the emitted neutrino [1,2].

3.2.3 Gamma Emission

Gamma radiation is a high-energy electromagnetic radiation that exceeds the energy of most x-ray radiation. The electromagnetic spectrum displayed in Figure 3.2 shows the different electromagnetic waves starting with radio waves which have the longest wavelength and ending with gamma rays with the shortest wavelength. The gamma radiation is emitted from the nucleus in the form of high energy photons and they act more like particles than waves. The gamma photon has no mass or charge and does not change the atomic number or mass number of the atom. The equation that best describes the gamma decay is

$$X_Z^A \rightarrow X_Z^A + \gamma, \tag{3.4}$$

where the gamma emitted is represented by γ [31].

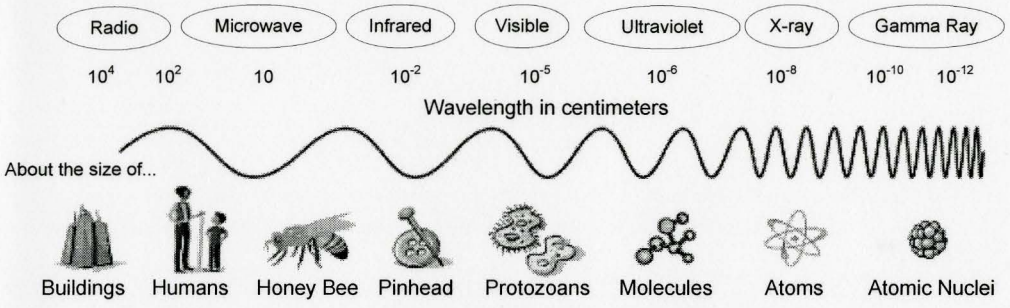

Figure 3.2: Electromagnetic Spectrum [35]

Gamma radiation is emitted when the nucleus is in an exited state. Both stable and unstable nuclei can be in an exited state, where they would have excess energy. Sometimes the de-excitation of a nucleus occurs by the emission of an alpha, beta, neutron or a proton, but most frequently it takes place by the emission of gamma photons. Typically the excitation of the nucleus occurs after its parent nucleus had gone through an alpha or beta decay [34]. The following example outlines this type of excitation:

$$Co_{27}^{60} \rightarrow Ni_{28}^{60*} + \beta^{-} \quad \text{(Beta emission)} \tag{3.5}$$

$$Ni_{28}^{60*} \rightarrow Ni_{28}^{60} + \gamma \quad \text{(Gamma emission)}, \tag{3.6}$$

where the asterisk represents the nucleus in an excited state. In this case, the Cobalt-60 went through beta decay and became a Nickel-60 with excess energy. Therefore the Nickel-60 had to undergo another decay, a gamma decay, in order to reach a ground level state of energy. However latter decay takes place very shortly after the former, since the maximum duration of a nucleus being in its excited state is 10^{-9} s [31].

3.3 Radiation and Materials

Ionizing particles are ones that carry electric charge and result in surrounding atoms to become ions. Alpha and Beta are considered ionizing particles since they both carry charge; a charge of +2 for alpha particles and either a -1 or +1 for the beta depending on its type of decay. Gamma Photons, on the other hand, are classified as indirectly ionizing since they are not ionizing themselves, but cause the emission of ionized particles from other atoms (i.e. secondary emissions) [31]. A summary of the characteristics of these three types of radiations is presented in Table 3.1 in this chapter.

3.3.1 Alpha Interaction with Matter

Alpha particles are heavy and can only penetrate short distances in matter. They can be stopped by a sheet of paper and their range of travel in air is 1 cm for every 2 MeV [36]. Their interaction with electrons in a material is what prevents them from traveling far; their speed is reduced due to the attraction forces between them and the surrounding electrons. However, they are energetic particles and their ionization of surrounding atoms is immense. In one centimetre, an alpha particle can create approximately 50 000 ion-pairs in dry air [31].

Ionization of the surrounding atoms in a material occurs when the alpha particle is relatively slow and close to their electrons. However at its final stage of interaction with matter, the helium ion gives the orbiting electrons time to detach from their atom and get captured by it. Eventually the ion adopts its two complimentary electrons, gives some of its remaining energy to nearby atoms, stops, and becomes a neutral helium atom. This transform of energy is what causes other atoms to be in an excited state [31]. Table 3.1

(in page 58) shows the alpha particle's energy range, and propagation range in air and tissue.

3.3.2 Beta Interaction with Matter

The penetration of beta particles through matter is typically much higher than alpha particles. The difference in penetration depth is associated with the fact that electrons are lighter than alpha particles [36]. On the other hand, beta particles cause less ionization to the surrounding ions for the same traveled distance when compared to alpha particles. In dry air, they can generate 100-300 ion-pairs for every centimetre propagated [31].

3.3.3 Gamma Interaction with Matter

Gamma rays have no charge and no mass, which makes them non-ionizing to surrounding atoms. They are different in their interaction with matter when compared to alpha and beta particles. There are three fundamental ways of gamma rays interaction with matter, namely the photoelectric, pair production, and the Compton effect.

3.3.3.1 The Photoelectric Effect

This effect occurs when a gamma ray of low energy strikes an orbiting electron, transferring all its energy to the electron (and some to the atom). The gamma ray disappears, while the electron detaches from the atom and behaves like a beta particle as shown in Figure 3.3. The electron, called the photoelectron in this case, receives the energy from the photon in the form of kinetic energy less the binding energy and the little kinetic energy given to the atom. If the electron released is an inner atomic electron, it leaves a hole in the structure. The hole is then filled by an outer electron, creating

another hole that is filled by another outer electron. It keeps occurring until the hole reaches the outermost atomic orbital shell. During this transition process of filling holes by outer electrons, either X-rays are emitted or other electrons are ejected, known as Auger electrons [32].

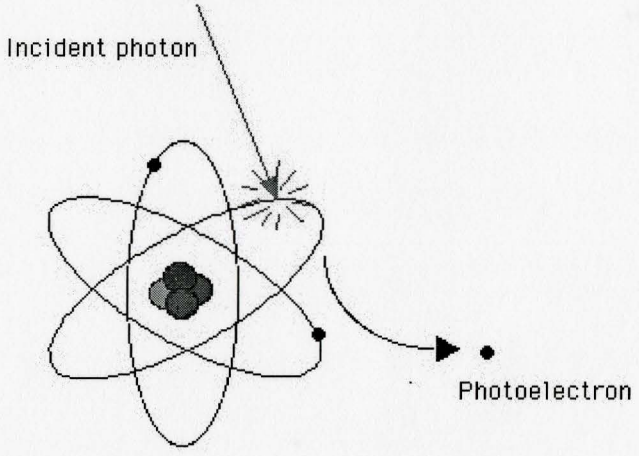

Figure 3.3: The Photoelectric Effect [37]

3.3.3.2 Pair Production Effect

The pair production effect occurs only when the gamma photon is in the vicinity of an atomic nucleus, where there is a Coulomb field. When an incident gamma photon with high energy comes close to a nucleus, it transforms its energy into creating an electron-positron pair (as shown in Figure 3.4). For this effect to occur, the gamma photon has to have a minimum energy of 1.022 MeV; this is equivalent to the mass energy of two electrons at rest. The kinetic energy received by both the electron and positron is equal to the energy of the photon less 1.022 MeV [31].

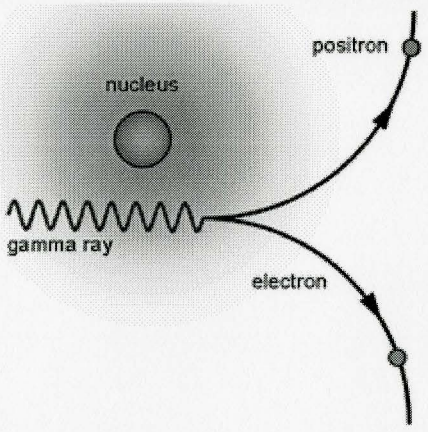

Figure 3.4: Pair Production Effect [38].

The positron and electron then cause ionization and lose their energy along the way as described earlier in the beta emissions section. Eventually, as the positron slows down, it combines with another atom's orbiting electron and they both cease to exist. As shown in Figure 3.5, two gamma photons of 0.511 MeV energies are then released as a result of this annihilation process. This is known as an annihilation radiation, where the gamma photons can cause further interactions [32].

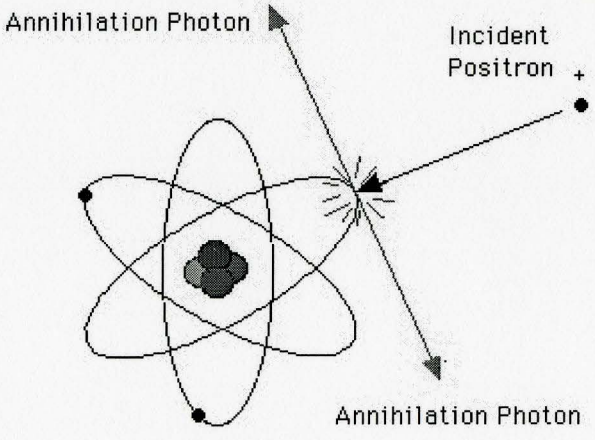

Figure 3.5: Annihilation Radiation [39]

3.3.3.3 The Compton Effect

This type of interaction typically occurs when the gamma photon's energy ranges between 0.1 and 10 MeV [31]. The gamma photon strikes an orbiting electron, then gets scattered into a different direction (see Figure 3.6). The electron, known as the Compton electron, receives enough energy from the gamma photon to detach from its atom and becomes an ionizing beta particle. The scattered gamma photon has lost some of its energy, and therefore has a different wavelength; in fact it has a larger wavelength according to the following energy-wavelength (E-λ) relationship

$$\lambda = \frac{hc}{E}, \tag{3.7}$$

where h is Planck's constant and c is the speed of light. The scattered gamma photon can then be thought of as a different gamma photon emitted after the incident gamma photon was absorbed by the Compton electron.

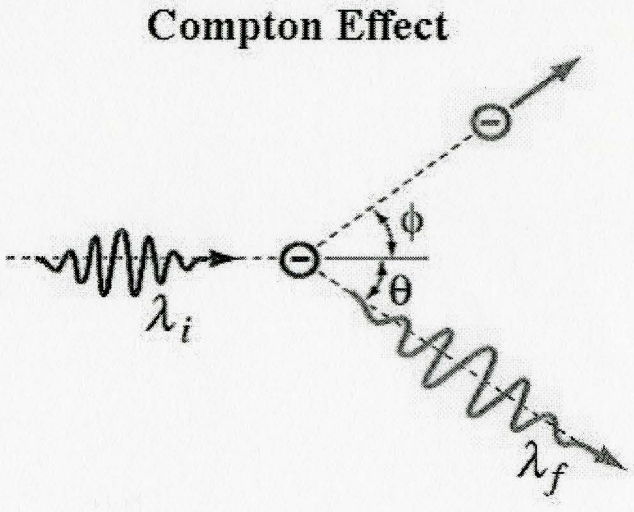

Figure 3.6: Compton Effect [40]

The Compton Effect has caused many problems in the shielding of gamma radiation. Unlike the photoelectric and pair production effect, the gamma photon does not vanish after its first encounter. In fact it goes through a series of such an interaction before it becomes a low energy photon that can be absorbed by the photoelectric effect. Although, as mentioned earlier, X-rays and Auger electrons are emitted immediately after the photoelectric effect, and gamma emissions (Annihilation radiation) occur towards the end of the pair production effect, they are significantly less energetic than the original gamma photon. They do not penetrate as deep in matter as the Compton scattered photons do [32].

3.4 Neutron Interaction with Matter

Neutrons are emitted from atoms as a result of different reactions and processes, such as nuclear fission, nuclear fusion, and very high energy reactions. There are two ways in which neutrons react with nuclei, through scattering, and absorption. Both reactions occur in two stages; the first stage is the capturing of a neutron, and the second is the emitting of a particle. A neutron is captured by a (stable or unstable) nucleus, creating a compound nucleus in an excited state. Shortly after, the compound nucleus either emits a particle, which can be a neutron if it is a scattering interaction, an alpha particle, a proton, or a gamma photon, or splits into two parts (fission) [31].

The binding and kinetic energies resulting from the captured neutron are what give the targeted nucleus extra energy that sets it in an excited state. The amount of energy received by the nucleus during its interaction with the neutron, as well as the type of target nucleus, determines the second stage of the reaction [31].

3.4.1 Scattering Interactions

The study and analysis of neutron scattering interactions is essential for the design of the nuclear reactor. Neutron scattering interactions reduce its kinetic energy allowing it to undergo further and different interactions, such as absorption, when it reaches desired energy levels. This method of energy reduction is referred to as moderation.

3.4.1.1 Inelastic Scattering

In inelastic scattering interactions, a fast neutron is captured by a nucleus and another neutron is emitted with a lower kinetic energy, leaving the nucleus in an excited state. The kinetic energy from the captured neutron is either fully or partially given to the excitation of the nucleus. Gamma photons, equivalent to the excitation energy, are then emitted from the nucleus in order for it to go back to its ground energy level. The following equation describes this process in terms of energies:

$$E_1 = E_2 + E_\gamma, \tag{3.8}$$

where E_1 represents the total kinetic energy of the neutron and nucleus before the collision, and E_2 after the collision, while E_γ symbolizes the energy emitted in the form of gamma photons. For an inelastic scattering to occur, E_1 must at least exceed the energy of one photon, which is the minimum value that E_γ can have and the minimum excitation energy a nucleus can reach.

Inelastic scattering may also take place with nuclei that are bombarded by low energy neutrons. This type of scattering occurs when the nuclei targeted are bound to a molecule or are in their solid form. These nuclei tend to have discrete quantum states created as a result of the atomic vibrations in molecules or solids. When the low energy

incident neutron collides with the bound atom, it changes these quantum states leading to either an increase or decrease of internal energy. However in this case, there is no formation of a compound nucleus, and the emitted neutron may have a kinetic energy greater than the captured one [31].

3.4.1.2 Elastic Scattering

Unlike inelastic scattering collisions which are restricted to a certain range of high or low energies in their interactions, elastic scattering have no limitation to their exchange of energy between the neutron and the targeted nucleus. Regardless of the nucleus's condition (bound or free), neutron elastic scattering interaction can occur at any energy with the nucleus. Moreover, kinetic energy is conserved in this type of scattering interaction, since there is no change in system's internal energy. The total kinetic energy before and after the collision is always equal, where if any change in energy occurs to one of the parties (neutron or nucleus) after the collision, the same change would apply to the other party.

There are two types of elastic collisions, namely the potential scattering and resonance scattering. Potential scattering occurs when a low mass nucleus is approached by a neutron traveling with energy of a few MeV. Scattering, in this case, occurs as a result of short-range potential forces that act on the approaching neutron, and no compound nucleus is formed. The resonance scattering, on the other hand, forms a compound nucleus as the incident neutron collides with the nucleus. A neutron is then emitted from the nucleus with lower kinetic energy, giving the nucleus some of its kinetic

energy while leaving it at ground state of excitation level. This type of collision abides by the laws of conservation of kinetic energy and momentum.

Eventually, the neutrons exhibiting successive elastic scattering collisions lose their speed (kinetic energy) and reach the average kinetic energy the atoms in the medium have. They reach thermal equilibrium with the atoms, where their energy depends on the temperature of the medium [31].

3.4.1.3 Neutron Absorption Reactions

There are a few types of neutron absorption reactions that occur after the formation of a compound nucleus. As a neutron is captured by the target nucleus, there is a possibility of an emission of another neutron; however it is not always the case. The energy gained by the nucleus and how it is distributed amongst the nucleons is what determines the aftermath. The energy needed for a single neutron to be emitted ranges between 5 and 8 MeV [31]. Therefore if the excitation energy of the compound nucleus is large and the number of nucleons sharing it is small, then there is a high probability that a neutron will be emitted. On the other hand, if a neutron emission does not take place, one of the following reactions will take place: gamma photon emission (n, γ), alpha particle ejection (n, α), proton ejection (n, p), or fission (n, f) [31].

Radiative Capture Reactions (n, γ)

Radiative capture reaction is the most common reaction which occurs with a wide range of elements. This type of reaction is best described by

$$X_Z^A + n \rightarrow X_Z^{*(A+1)} \rightarrow X_Z^{(A+1)} + \gamma, \tag{3.9}$$

where X is the target nucleus with an atomic mass number A and atomic number Z, the asterisk indicates the nucleus in an excited state and γ resembles an emission of gamma photons. In this case, the excitation of the nucleus is relieved in the form of gamma photons, leaving the nucleus at a potentially radioactive state. If the resulting nucleus is radioactive, then the following decay is most likely negative-beta decay, since its neutron to proton ratio is larger than the stability ratio pertaining to the specified element. With the exception of a few magic number nuclei, all elements undergo radiative capture [31].

Emission of Alpha Particles and Protons

It is rare for a positively charged particle to be emitted from a nucleus after a slow neutron capture. In order for an alpha particle or a proton to be ejected, it has to receive enough energy to overcome the columbic forces (electrostatic potential) in the atom on top of the energy associated with the detachment of particles from the nucleus. On the other hand, during fast neutron interactions, the probability of the ejection of these particles is higher than the emission of gamma radiation. In the case of higher neutron energy levels striking a nucleus, more than one proton or neutron can be ejected from the compound nucleus. However the probability of fast-neutron reactions is small, which makes them not as essential to the study and design of nuclear reactors [31].

The Fission Process

The excitation energy received by the compound nucleus as a result of the absorption of the neutron, leads to a series of oscillations in the nucleus. If the energy from the oscillation is sufficient, the nucleus undergoes a fission process, where the nucleus is split into two separate nuclei. The liquid drop model of the atomic nucleus is

very helpful in describing this process. According to this model, the steps in which a nucleus (a drop) goes through until the actual split of the nucleus is briefly shown in Figure 3.7.

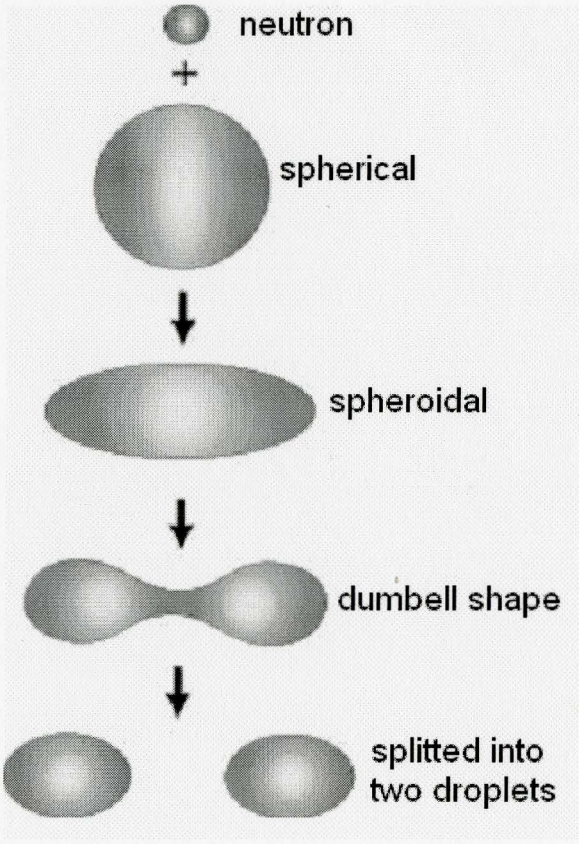

Figure 3.7: Liquid Drop Model of Fission [41]

3.4.2 Lattice Displacement Damage

Particles bombarding a solid material either undergoes ionizing or non-ionizing processes as they propagate through the material. In the case of ionizing effects, electron-hole pairs are created, whereas, when it is a non-ionizing interaction, atoms are displaced in the lattice. Displacement damage is a lattice defect that includes the creation

of vacancies and interstitials in the structure. A vacancy occurs when an atom is absent from its normal lattice position, and an interstitial is when the absent atom resides in a non-lattice position. Once these defects are created, they reorder to form more stable formation [52].

The degree of radiation induced damage depends on several factors, such as the particle type, particle energy, irradiation temperature, measurement temperature, time after irradiation, thermal history after irradiation, injection level, material type, and impurity type and concentration [52]. The general sequence of events that causes materials and devices to degrade are as follows: 1) incident particles displace; 2) the resulting defects give rise to new energy levels; and 3) those levels alter material and device electrical and optical properties. Any disturbance to the periodicity of the lattice may give rise to energy levels in the bandgap, which leads to one or more of the following processes: generation, recombination, trapping, compensation, tunnelling, scattering, type conversion, and field enhancement of carrier generation effectiveness [52].

3.5 Radioactive Shielding

Radiation shielding is used for different functions. It could be used to protect humans from the radiation exposure (biological shielding), to protect vessels on a nuclear reactor from heating due to gamma ray absorption (thermal shields), or to protect electronic devices that malfunction when exposed to radiation (apparatus shield). Typically shields are necessary for gamma rays and neutrons. This is because other radiations, like alpha and beta particles, propagate very short distances in matter. Table

3.1 shows the properties of each type of radiation, including their range in air, tissue, and their shielding requirements [31].

Table 3.1: Properties of Types of Radiation [42]

Type of Radiation	Atomic Mass Unit (AMU)	Charge	Energy Range (MeV)	Range in air (cm)	Range in tissue (mm)	Shielding
A	4	+2	4 to 8	2-8	0.04	Paper
B	~0.0005	-1	0.1 to 3.5	15-1600	5	Low Atomic No.
Γ	0	0	Up to 10 (most below 3)	1300-13000 (HVL)	Through Body	Lead or High Density
Neutron	1.008665	0	0-10		Through Body	Hydrogen Containing Substance

Chapter 4

Literature Review on the Effects of Nuclear Radiation on SAW Devices and other Quartz Resonators

4.1 Introduction

Very few papers have been published on radiation effects on SAW devices, when compared to quartz resonators. The most recent paper on SAW devices and radiation effects was published in 1991 [43,45]; however, work in the field has been done recently on Quartz crystal resonators [44]. In this chapter, a general review of previous experiments conducted on SAW devices and quartz resonators under nuclear irradiation will be presented along with some interpretations of their results.

4.2 Ionizing Radiation Effects on SAW Resonators

J. H. Hines and W. J. Stapor published the most recent papers regarding this subject [43,45]. They have investigated the operation of different types of SAW resonators with very high Q and narrowband under the exposure of space-like radiations, like gamma, high energy electron, and proton radiation. They claim that conclusions drawn from previous researchers on the same matter are generalised and do not encompass all types of SAW devices. Their conclusions were that all SAW devices are not severely affected by ionizing radiations; however, Hines, Stapor, and Wilson prove in

their papers that SAW devices such as resonators and filters with narrow passband frequency response are relatively sensitive to radiation.

In their experiments, they used SAW resonators with a centre frequency of 199 MHz, a narrow bandwidth (21 kHz), and a high Q (10,000). Three different configurations of this highly sensitive SAW resonator were experimented; some of which were fabricated on air-swept quartz, some on non-swept quartz, and the rest were non-swept with SiO_x surface coating. Non-swept devices have substrates fabricated with commercial electronic grade quartz which innately includes a number of impurities. Air-swept quartz devices, on the other hand, have a lower concentration of impurities as a result of a special purifying (sweeping) process performed on the substrate. Ten different parameters have been measured on the resonators before and after the irradiation, including insertion loss, device Q, centre frequency, 3 dB bandwidth, and other frequency and phase measurements taken at different events. In addition, there were a few selected control devices that were not exposed to radiation, and were used to monitor any parameter changes due to external factors, whether environmental or circuit-based, that needed to considered. Thus, they made sure that the shift in parameters was solely due to the changes in radiation dose. At each level of radiation, they used 4 control and 4 target devices [45].

The results, as shown in figures 4.1, 4.2, and 4.3, indicate a drastic shift in frequencies have occurred with non-swept quartz devices, especially under gamma and proton radiations, as opposed to relatively small changes with air-swept and non-swept coated devices. The other parameters have been measured, but since their changes were

not as significant as the frequency changes with regards to SAW resonator applications, not much emphasis was put on them. In the case of swept quartz substrate devices, a negative change in frequency has occurred for all types of radiations used and all levels of radiation doses measured at. The maximum negative change reached for this type of resonator, for a total dose of 10 Mrad(Si), was 20 ppm.

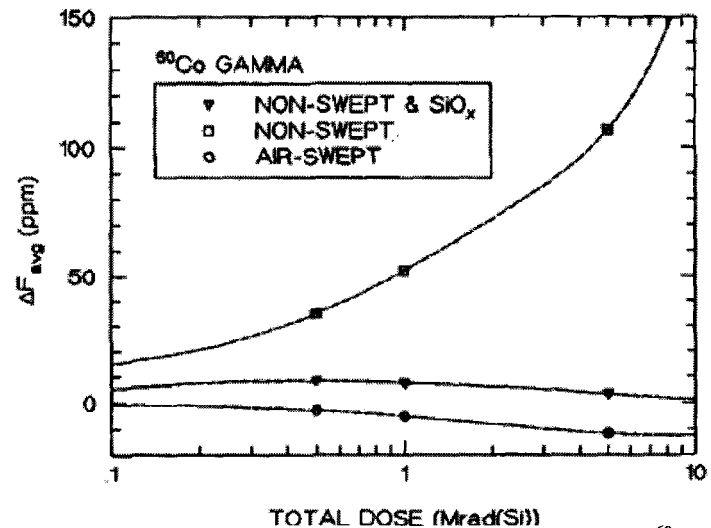

Figure 4.1: Frequency Shift (in ppm) versus Total Dose (in Mrad(Si)) from ^{60}Co Gamma Radiation [43]

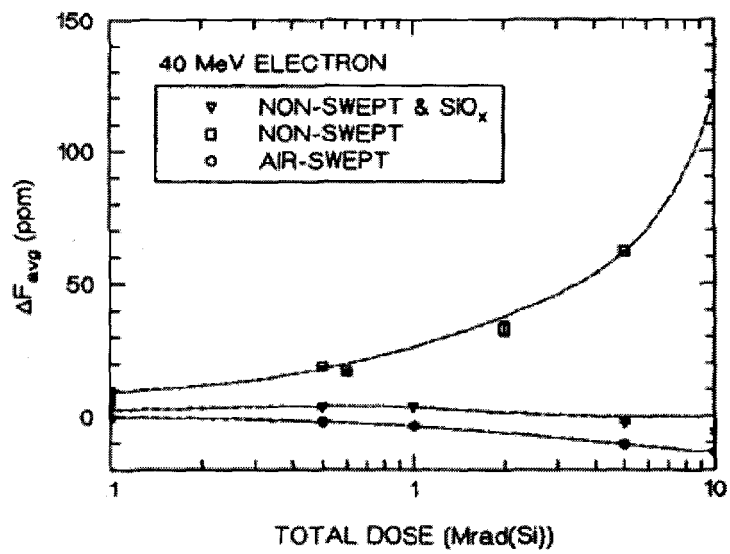

Figure 4.2: Frequency Shift (in ppm) versus Total Dose (in Mrad(Si)) from 40 MeV Electron Radiation

[43]

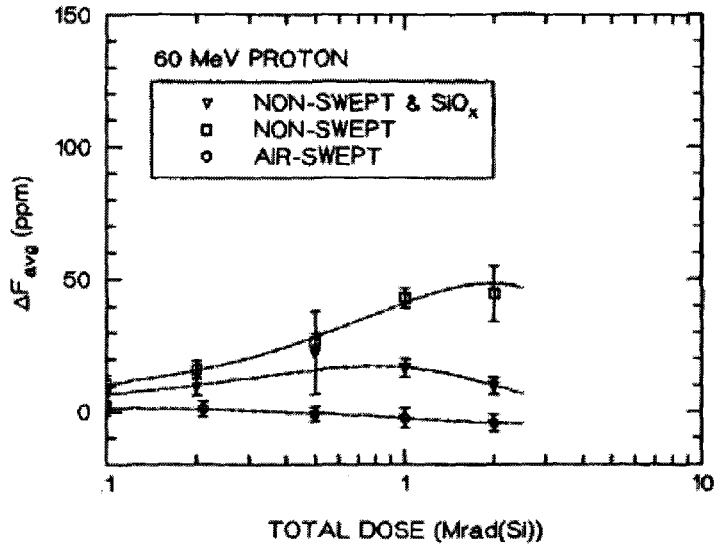

Figure 4.3: Frequency Shift (in ppm) versus Total Dose (in Mrad(Si)) from 60 MeV Proton Radiation [43].

Under the three different types of radiation, the non-swept quartz resonator underwent very large positive frequency shifts, when compared to the air-swept devices. It reached a shift of 120 ppm at 10 Mrad(Si) dose for electron radiation, and above 150 ppm for gamma radiation (at 10 Mrad(Si)). Such large changes in parameters would drastically affect the performance of these devices (made of non-swept quartz) if subjected to as high levels of radiation dose. Therefore for long-lasting space orbiting systems, these devices would not be recommended.

Non-swept SiO_x coated devices resulted in a complicated trend of frequency shift as the radiation dose increased. Until an accumulated dose of 0.6 Mrad(Si), the frequency change was increasing positively. It then started decreasing, until it crossed zero at 2.5 Mrad(Si) and began going negative. With the aid of previous papers published on radiation effects and quartz, Hines et al. explained the increase and decrease of frequency shift to be a result of radiation stress at the early stages of radiation that

turned into radiation compressions after a certain dose level. The addition of the SiO_x had added stresses to the substrate, which were released by smaller doses of radiation, resulting in the positive frequency change. Subsequently, the negative change occurred due to the further radiation damage to the substrate that had caused compression of the material.

Hines and Stapor's interpretation to the effect of radiation on SAW devices or quartz substrates in general is presented as follows: The radiation reaching the substrate causes displacement and ionization damage to its surface. Such damage to the surface perturbs the propagating acoustic wave, changing its phase velocity. With added amounts of radiation to the surface, more damage and more velocity change take place. However, as they claim, some self-recovery of the surface material occurs after the damage to the structure of the material is incurred. They have come up with an expression that best fits the trends of each type of device under all three types of radiation, taking into account recovery processes, as follows:

$$\Delta F_{avg} = A\exp(B\Phi)(1 - C\exp(-D\Phi)). \tag{4.1}$$

In this expression, ΔF represents the frequency shift (in ppm), Φ denotes the total accumulated dose (in Mrad(Si)), and A, B, C, and D are fitting parameters that vary with the type of resonator used and radiation applied (Table 4.1 lists the parameter values that were induced for their results) [43]. The first term in this equation signifies the substrate's damage (in terms of exponential frequency change), while the second term represents its recovery.

Table 4.1: List of Parameter Fitting Values for the Derived Frequency Shift Expression, reproduced from [43].

RADIATION & RESONATOR	A	B	C	D
^{60}Co γ Air-swept	13.44	-0.470	1.004	-0.463
^{60}Co γ Non-swept	64.30	0.102	0.868	1.174
^{60}Co γ Non-swept & SiO_x	9.33	-0.203	0.998	8.277
e^- Air-swept	10.49	-0.406	0.988	-0.435
e^- Non-swept	32.03	0.133	0.797	1.043
e^- Non-swept & SiO_x	201.20	-1.509	0.993	0.075
p Air-swept	26.84	-0.515	0.922	-0.228
p Non-swept	800.20	-0.461	0.994	0.079
p Non-swept & SiO_x	442.90	-1.130	0.995	0.120

4.3 Radiation Effects on other Quartz Resonators

Other quartz resonators have been investigated under different types of radiation as well as conditions. Thermosensitive quartz crystal resonators have been examined under fast neutrons and gamma rays. Gamma irradiation was applied on these resonators at room temperature, while neutron induction took place at both, liquid nitrogen and room temperatures, respectively [46]. The grown quartz substrate in the devices used included Aluminium, Sodium, and Lithium content. Minor changes in the properties of the resonators, which were detected by shifts in the resonating frequency as the dose

increased, had been explained to be a result of the impurity defects present in the substrate.

The frequency of the devices that were exposed to gamma radiation was measured after different radiation doses, ranging from 1 Mrad to 5 Mrad(Si) with measurements taken every 1 Mrad. As presented in Figure 4.4, there is an overall decrease in frequency until a saturation point is reached (approximately of -8 ppm at 3 Mrad(Si)), where the negative change rapidly slows down and becomes constant. However, at lower doses of up to 0.5 Mrad(Si), a slow positive increase in frequency was taking place, and the authors explained it to be as a result of relaxation processes, surface strain, dissociation or relaxation effects in the electrodes as well as the crystal holders [46].

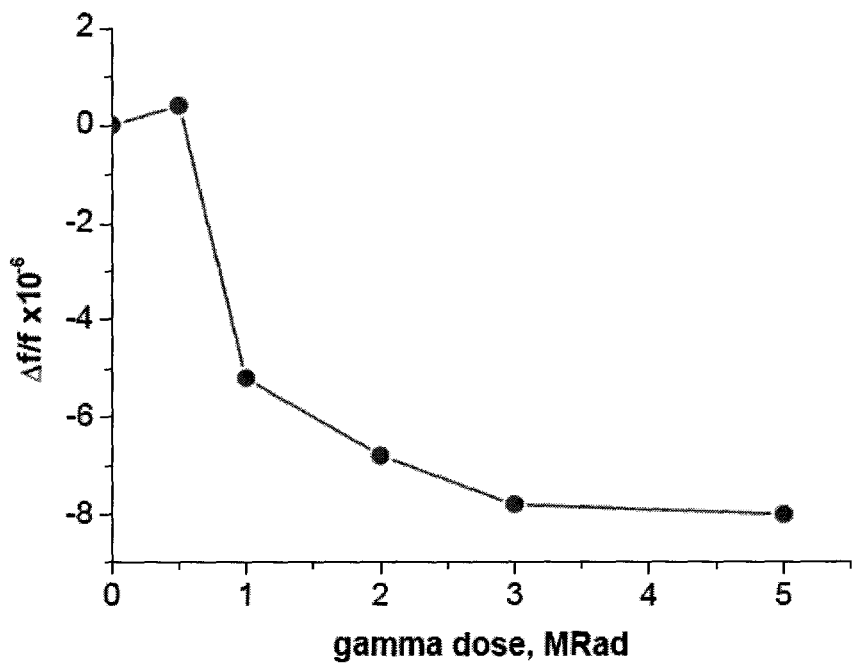

Figure 4.4: Influence of Gamma Radiation on Resonance Frequency [46].

In the case of neutron irradiation of these devices, two different conditions were examined; namely, room temperature and extremely low temperature (liquid nitrogen).

For almost the same range of radiation dose examined, a significant difference in frequency shifts was found when comparing results from both conditions. However, as explained by the researchers, it is mainly due to the temperature induced instability of the resonators. There was no defined trend in both conditions; a random and inconsistent change in frequency was seen for an increased neutron dosage. Figure 4.5 displays the results taken from devices exposed to neutron radiation at room temperature.

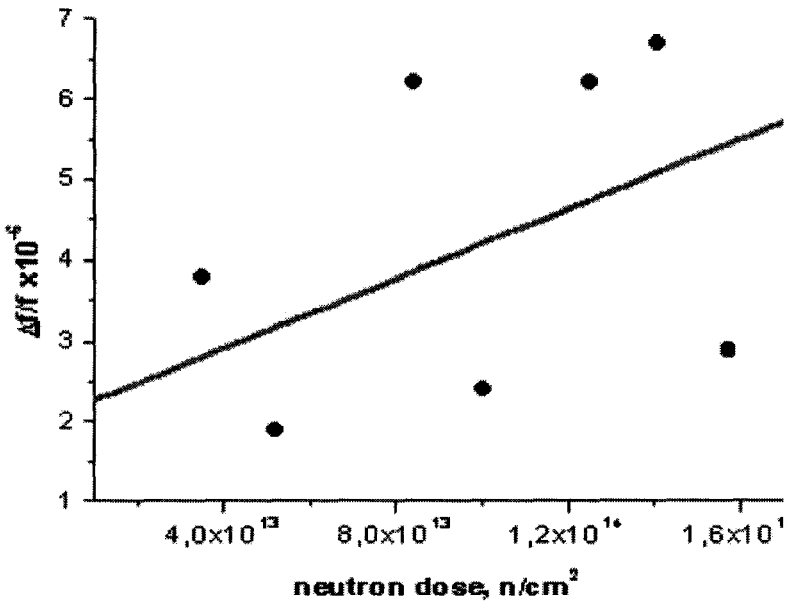

Figure 4.5: Neutron Dose Effect on Resonance Frequency at Room Temperature [46].

A paper published in 1987, observed the effect of Aluminium impurity concentration under gamma radiation [47]. It was shown that there was greater device sensitivity at low radiation doses (3 to 5 x 10^{-11} per rad) when compared to shift in frequency at medium radiation dose accumulation (5 to 20 x 10^{-13} per rad). Aluminium impurity concentrations effect was not evident at low dose levels; however at total accumulated doses exceeding 1000 rads, it started to appear. Greater Aluminium

impurity content in the quartz substrate, led to greater frequency shifts and recovery periods of the device.

Other experiments conducted on quartz devices being exposed to gamma and proton radiations, allowed some authors to conclude that electrode deposition processes endorse radiation-induced changes through surface relaxation [44]. However in the paper published by M. Flanagan et al, the authors deduced that changing mass on the surface of a substrate is not what causes the frequency shift during irradiation. In fact, they explained such changes to result from electric fields created due to induced trapped charges. On the other hand, other researchers in the field believe that these conclusions were drawn without the consideration of other possible effects. There is a possibility of stress created by entrapped impurities under the electrodes or by adhered gold thin films that are relaxed when radiation is applied. This makes M. Flanagan et al's interpretation of the matter incomplete.

An older paper investigated the effect of gamma radiation on the dielectric properties of quartz [48]. Using a ^{60}Co as the gamma irradiation source, significant increase in the dielectric loss angle and permittivity were detected. G.I. Potakhova explained that such changes occur as a result of the absorption of gamma rays by the substance through Compton scattering. Compton electrons are created in the quartz, where they go through more interactions with the atoms in the substrate, polarizing them; in turn altering the electrical properties of the substrates.

Chapter 5

SAW Resonator Irradiation

5.1 Introduction

This chapter presents three experiments conducted on identical quartz resonators. The first experiment was to examine the effects of very high gamma irradiation on the device performance. The second one focused on investigating the frequency shifts of the devices up to 5 Mrad(Si) (50 kGy), which allowed comparison with previously published papers. The third experiment was performed to investigate neutron irradiation effects on another set of these devices. The first and third experiments were never done before; no papers have been published on irradiating SAW resonators up to very high gamma doses (50 Mrad(Si) or 500 kGy) to observe device breakdown, or solely on irradiating these devices with neutrons.

5.2 SAW Resonator

The device used in the experiments is a 433.92 MHz SAW resonator manufactured by RF Monolithics, Inc (RP1308 model). It is a two-port resonator composed of a quartz substrate and other materials used in its components, such as its IDT, lid, and wires (Table 5.1 lists the different materials used in the RP1308 resonator). The device is packaged in a low-profile TO39-3 case with three pins, as shown in Figure 5.1, and weighs 0.822 grams. Each device provides a reliable and stable centre frequency f_c that ranges between 433.845 and 433.995 MHz differing from one device to the other;

where when part of an oscillator, the oscillation frequency $f_{oscillation}$ is less than f_c. It has a typical insertion loss of 6.3 dB and an unloaded Q value of 12,000. Its temperature characteristics are graphically shown in Figure 5.2 [49].

Table 5.1: List of Materials in RP1308 SAW Resonator Model

Material	*Substance*	*Per Part Wt*	*Per Part %*	*Per Material %*
Header	base iron	0.3116282	37.9%	51.5%
	base nickel	0.1763933	21.5%	29.1%
	base cobalt	0.0999562	12.2%	16.5%
Plating	nickel plate	0.0029374	0.4%	0.5%
	gold plate	0.0007222	0.1%	0.1%
	glass seal	0.0138921	1.7%	2.3%
Lid	base iron	0.1074832	13.1%	51.3%
	base nickel	0.0608395	7.4%	29.0%
	base cobalt	0.0344757	4.2%	16.5%
Plating	nickel plate	0.0067316	0.8%	3.2%
Die (SAW)	Quartz	0.0060970	0.7%	99.94%
	Aluminum	0.0000038	0.000%	0.06%
Die Attach	AlN	0.0003219	0.04%	67.0%
	resin	0.0001585	0.02%	33.0%
Bond Wire	Aluminum	0.0000215	0.0026%	99.0%
	Silicon	0.0000002	0.000026%	1.0%
			99.9%	

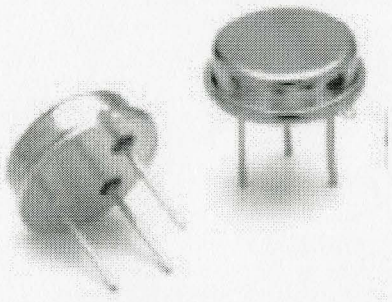

TO39-3 Case

Figure 5.1: TO39-3 Case [49].

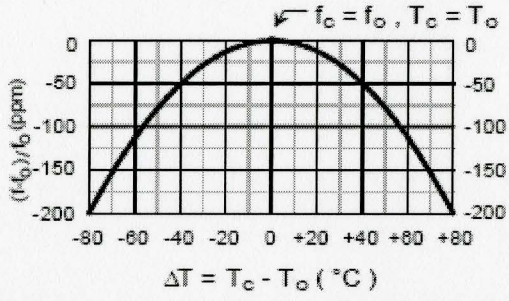

Figure 5.2: Temperature Characteristics [49].

The equivalent circuit of the SAW resonator is presented in Figure 5.3. The typical values of its motional resistance R_M, motional inductance L_M, motional capacitance C_M, and shunt static capacitance C_0 are as follows: 107 Ω, 481.378μH, 0.279470 fF, and 1.7 pF, respectively. This device could be either used as a two port or a one port, depending on its application. For the experiments presented in a later section, the one-port configuration was used as illustrated in Figure 5.4, where pins 1 and 2 are for input or output, and 3 for ground.

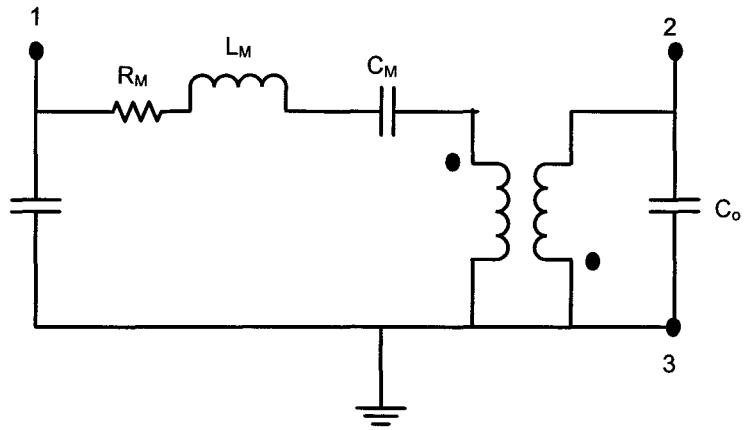

Figure 5.3: RF equivalent circuit of the SAW resonator [49].

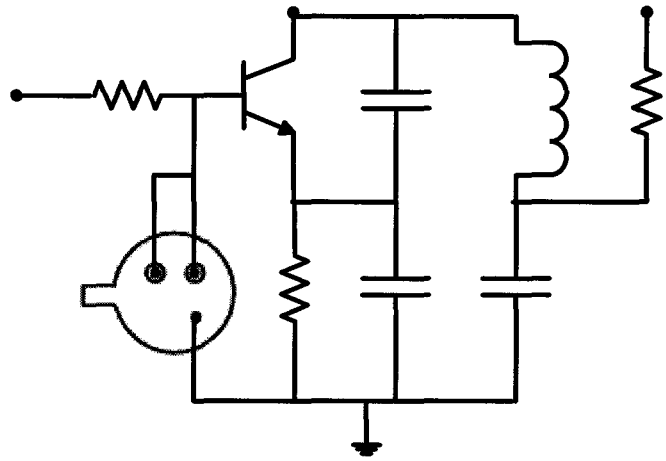

Figure 5.4: One-port SAW resonator Configuration in an Oscillator Circuit [49].

5.3 Oscillator

There are two conditions that must be satisfied for a circuit to become an oscillator:

1. A feedback loop gain of greater than 1. The amplifier in the loop must have sufficient gain to overcome the accumulated losses around the loop.
2. Total phase shift around the loop = $(\omega L/V_R) + \phi_e = 2\pi n$, where ω is the angular frequency, L is acoustic path length, V_R is the velocity of the acoustic wave, and ϕ_e is the phase change associated with the transducers and the electrons [10].

An oscillator was designed and built based on design notes on transmitters that have been recommended for the RP1308 SAW resonator [50]. Figure 5.5 shows the circuit design of the oscillator used, and the component values are displayed in Table 5.2. In order to change the design from a transmitter to an oscillator, a few modifications were made; the addition of

- A DC bias to the base of the transistor, and
- a capacitor C_p to the feedback loop; to allow the oscillation to be in phase.

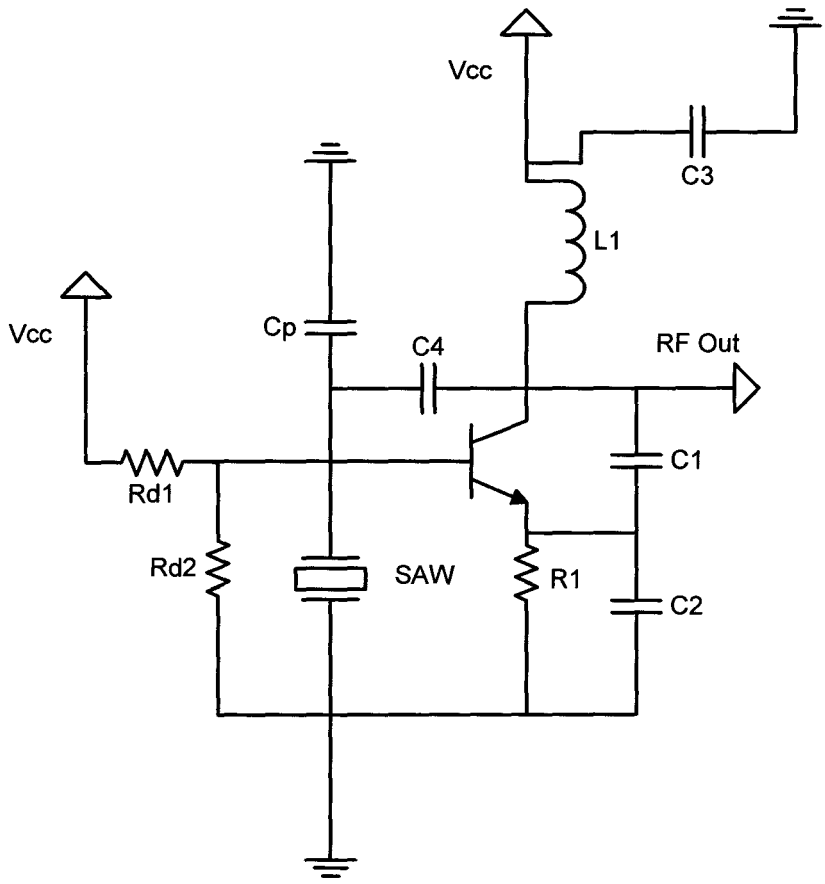

Figure 5.5: Oscillator Circuit for the SAW resonator [50].

Table 5.2: Component Values, reproduced [50]

Component	Value/Model
Transistor	NEC 2SC4228
C1	1-5.1 pF
C2	8.2-18 pF
C3	470 pF
C4	1 pF
Cp	1 pF
L1	18-33 nH
Rd1 & Rd2	1 KΩ
R2	100 Ω

An oscillation frequency measurement of a sample SAW resonator placed in the oscillator circuit is shown in Figure 5.6

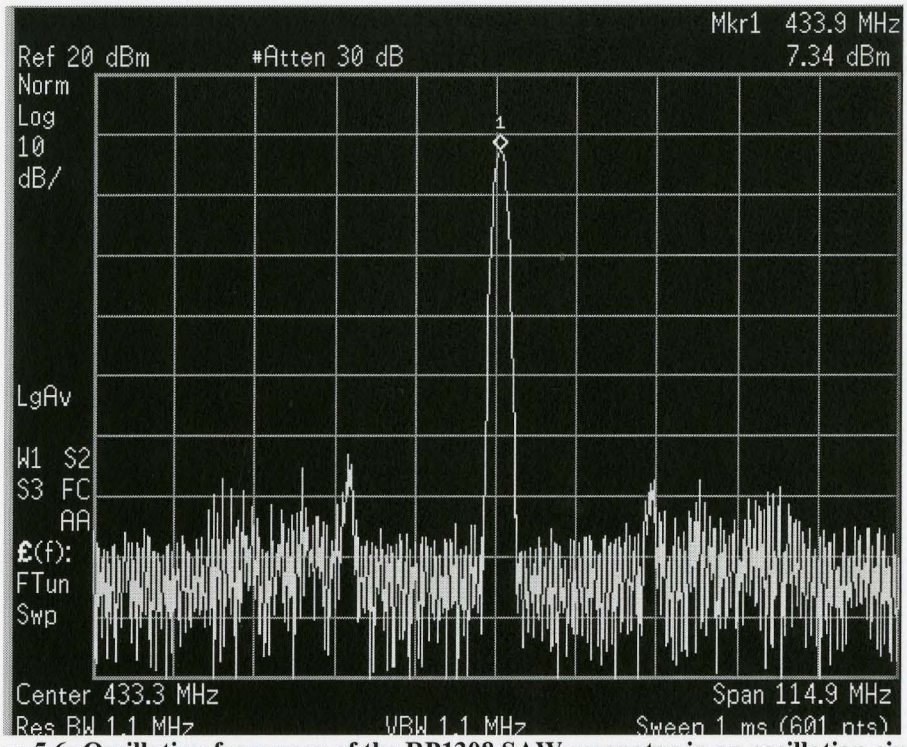

Figure 5.6: Oscillation frequency of the RP1308 SAW resonator in an oscillation circuit.

5.4 Experiment Procedure (Setup)

A PCB layout of the oscillator circuit, with the corresponding components soldered to it, was fixated firmly to prevent it from any movement. It was connected to a

spectrum analyzer through an RF coaxial cable, where once hooked, the setup was not touched until all the experiments were terminated. The SAW resonators were placed and removed carefully on the PCB board for measurements. All the resonators were tested and their frequencies were precisely measured before and after irradiation, and the changes in frequency were recorded. As has been mentioned in the literature [51], there is a ± 200 to ± 500 ppm difference from one device to another (same device) after the initial fabrication, due to variation between one substrate to another. Some processing variables cannot be fully controlled, such as the groove depth, metallization thickness, alignment of the device with the substrate, and the packaging.

For every experiment, one SAW resonator was kept as a control device, where it was not irradiated and mainly served as a detector of any frequency changes due to external factors. Any changes detected by these control devices were taken into account when calculating the changes in frequency of the irradiated devices. The experimented devices were measured right after their irradiation, unless they were radioactive for a certain period of time, to avoid any recovery effects.

Three experiments were performed on the SAW resonators; two using gamma and one using neutron irradiation. In the first experiment, SAW resonators were irradiated by gamma rays up to a total accumulated dose of 50 Mrad(Si) (500 kGy). This was done to observe the overall trend of frequency shift, as well as, to investigate if the device will malfunction at extremely high gamma exposures. The second experiment was mainly to study the trend of the frequency shift against gamma doses up to 5 Mrad(Si) (50 kGy), which makes it comparable to results previously published on similar SAW resonators or

other quartz resonators. Lastly, neutron irradiation of the resonator was examined also in terms of frequency shift. This experiment had a different setup and required that the devices to be left isolated after each exposure for a period of time, depending on its radiation exposure, until its radioactivity decayed to safe levels.

5.4.1 Gamma Irradiation setup

Both gamma irradiation experiments were performed at the McMaster Nuclear Reactor (MNR), where the gamma source was a single 'pencil' Cobalt-60 source as its schematic is shown in Figure 5.7. The gamma radiation that was given off was comprised of two photon energies (1173 keV and 1332 keV). The dose rate for the experiments was measured using a 0.6 cc ion chamber coupled with a corresponding dosimeter (essentially an electrometer for measuring the current from the ion chamber).

The resonators were fixed to a lab stand positioned beside the source, and the radius between them and the source determined the dose rate they were exposed to. In the first experiment, 20 resonators were being exposed to the gamma radiation, where every 5 Mrad(Si) of accumulated dose, 2 samples were removed from the source, brought to CRL, and measured using the spectrum analyzer. This process was repeated until the remaining 2 resonators had received 50 Mrad(Si). The radiation dose rate for this experiment was 579 rad/s (5.79 Gy/sec).

For the second gamma experiment, more focus was put on the trend of the frequency shifts, which required controlling more variables. Five samples were irradiated five times to reach an accumulated dose of 5 Mrad(Si), where each irradiation was up to 1 Mrad(Si) (dose rate of 57.9 rad/s). The same samples were used for all

irradiations, in order to avoid any inconsistencies in the fabrication of the SAW resonators. Otherwise the fact that the samples are not completely identical, which shows in the slight difference in their oscillation frequencies, would have to be taken into account when analyzing the results. In addition, to avoid any changes in the results due to recovery processes in the substrate, the samples were measured shortly after their irradiation session and returned immediately to the reactor after their measurement for the remaining irradiations.

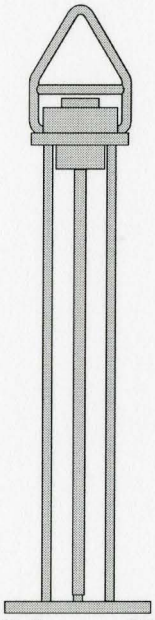

Figure 5.7: Schematic of the 'Pencil' Co-60 Source. The top (triangular part) is for hanging the source on the crane in the hot cell and the bottom part is where the gamma is emitted from [50].

5.4.2 Neutron Irradiation setup

The neutron irradiation took place in the Nuclear Research Building (NRB), through a system known as the "rabbit", which is directly connected to the MNR. Three resonators were placed in a plastic tube, where tissue was used as padding between them. The tube was placed in a pipe that connects between both buildings, in which it was accelerated and propagated into the core of the reactor. The travel time of the tube in the

reactor was set according to the amount of radiation desired, where the fluence (flux) was 4.5 x 10^{12} neutrons/cm^2.s (about 10% of flux is of fast neutrons). The tube with the resonators was then returned to the laboratory in the NRB and tested for radioactivity. Depending on their radioactive level, the tube was placed in a radiation insulated incubator for a certain period of time, ranging between 15 and 20 min. The samples were then brought to the CRL for measurements and returned right after to the NRB. This process was repeated 4 times until a 40 second worth of radiation accumulation (1.8 x 10^{14} neutrons/cm^2) had been received. This way, a comparison to previously conducted (neutron irradiation) experiments on quartz resonators is attainable.

5.5 Measurement Results

5.5.1 Gamma Results

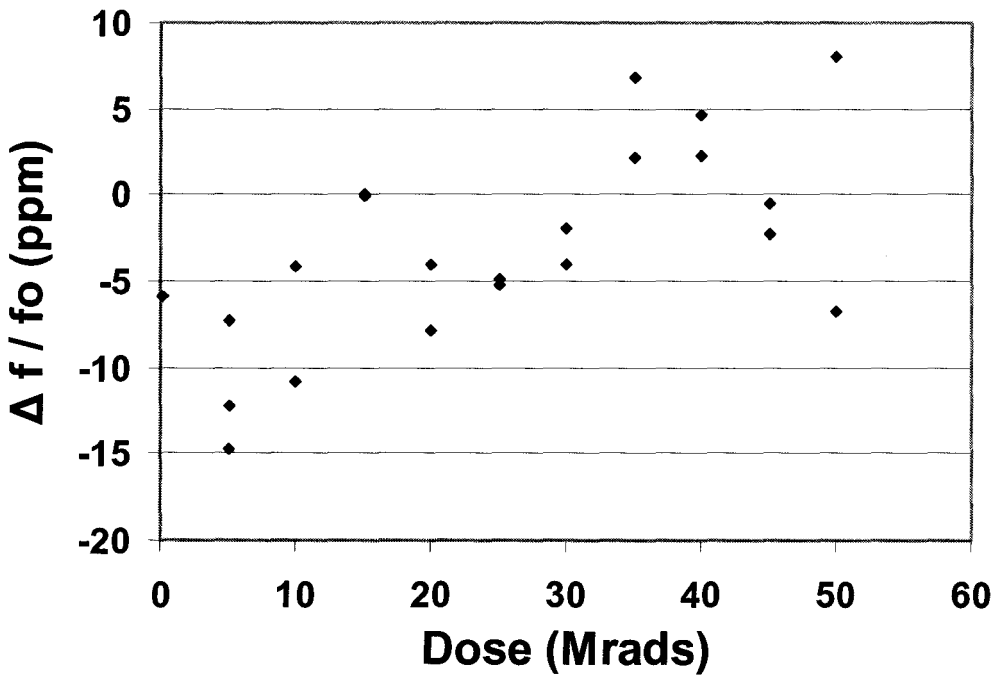

Figure 5.8: Results from gamma irradiation up to 50 Mrad(Si).

The results of the first experiment are displayed in Figure 5.8 and are tabulated in appendix 1. A few observations can be pointed out from the plot, and are as follows:

- The overall trend is completely random, even if the best fitted line between these scattered points was analyzed.
- For the same accumulated dose level, no two resonators exhibit the same change in frequency, except for two cases; at 15 and 25 Mrad(Si). In fact, in one case (at 50 Mrad(Si)), one resonator undergoes a positive change while the other goes through a similar change, but in the negative direction.
- Up to 50 Mrad(Si) (an extremely high gamma radiation dose), the resonators are still functioning, with a maximum change in frequency of -14.7 ppm attained at 5 Mrad(Si).

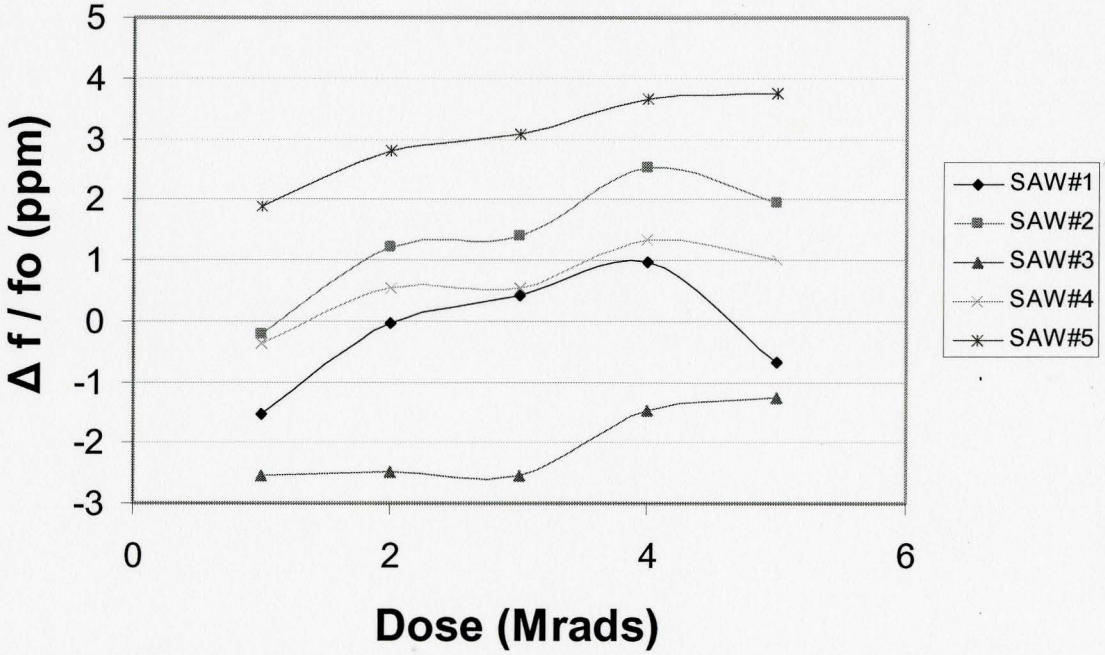

Figure 5.9: Gamma Irradiation up to 5 Mrad(Si)

Results from the second experiment, as plotted in Figure 5.9, show that each SAW resonator reacts different from the others under gamma radiation. Three of the five resonators underwent positive frequency changes, or at least for the majority of dose exposure levels. One completely exhibited negative frequency changes, and another started off with a negative change, then switched to positive changes, and then back to negative at 5 Mrad(Si).

If each resonator was analyzed separately, an attempt for explaining the results can be made based on conclusions drawn in previously published papers as presented in Chapter 4. But since each resonator acted differently, in terms of their sign of frequency change and frequency change trend, no general explanation can be deduced based on these results. The only useful observation, in this case, is that the maximum displayed change is 4 ppm at 5 Mrad(Si) (exhibited by SAW#5). Looking at both set of results from experiments 1 and 2, a conclusion can be drawn that the effect of gamma radiation on the SAW resonators, even at extremely high dose levels, is not significant enough to hinder their performance.

5.5.2 Neutron Results

The results of three SAW resonators being exposed to neutron radiation up to a total accumulated radiation of 1.8×10^{14} is shown in Figure 5.10. There is inconsistency in the frequency shift trends when comparing the three resonators as well as randomness in the plotted points when analyzing each resonator separately. The maximum frequency shift attained was 9.08144 ppm at 4.5×10^{13} neutrons/cm^2.s. These results agree with previous results published by researchers examining the effect of neutron radiation on

thermosensitive quartz resonators, as mentioned in chapter 4 when referring to paper [46]. The results are similar in terms of the randomness in the frequency shifts, as well as having the frequency shifts almost within the same range, except that all their results were in the positive region.

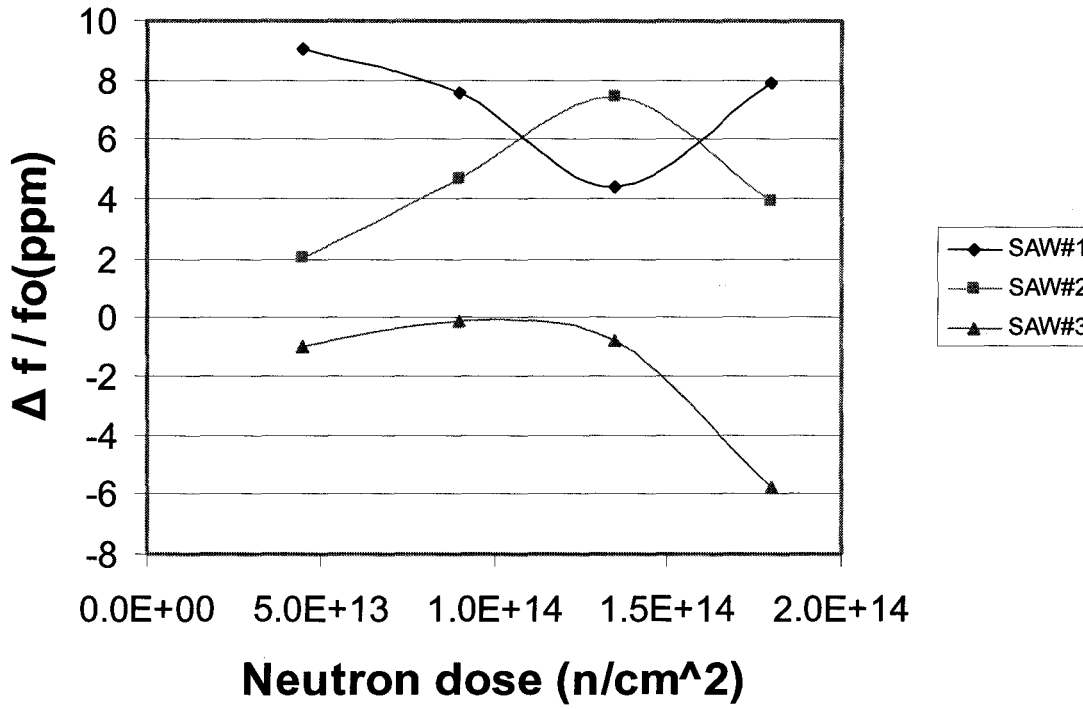

Figure 5.10: Neutron dose effect on resonance frequency of SAW resonators

Chapter 6

Conclusions and Future Work

6.1 Conclusions

In this thesis, several concepts have been discussed in order to establish the background needed for the experiments that were conducted. Acoustic Wave devices have been introduced in terms of their applications, various structures, application principles and architecture. Moreover, information on nuclear radiation was presented covering the different types of radiation, their creation, and effect on matter. Several papers regarding the radiation effects on quartz resonators, including SAW resonators, were reviewed and their conclusions were highlighted. Finally, the gamma and neutron irradiation experiments conducted on a RP1308 quartz SAW resonator with their various setups, procedures, and corresponding results were presented and analyzed.

Since gamma irradiation on SAW resonators has been investigated before, direct comparisons of results can be made. Although, the resonators used in this thesis are not exactly the same as the ones that have been previously experimented on in other papers, like [43] and [45], they were similar in terms of their very high Q and high operating frequency. The purpose of the first experiment was to observe any drastic change in the properties, or possible malfunctioning of the devices at extremely high dose levels, which are not normally attainable in years of earth orbiting in space. The devices have proven to withstand these very high levels of accumulated (absorbed) gamma radiation, with very little change in frequency reaching a maximum change of -14.7 ppm.

The second experiment, which can be directly compared to results from papers [43] and [45], focused on the frequency change trend of the resonators over a much lower dose level. The papers referred to above presented one type of their quartz SAW resonators, the non-swept quartz, to exhibit a maximum frequency shift of 110 ppm at 5 Mrad(Si). While this contradicts with our results for the gamma irradiation (0 to 5 Mrad(Si)), their other resonators, air-swept and SiO_x, experienced frequency shifts within the same range as our resonators. Our results enable us to conclude that commercially used SAW quartz devices, like the RP1308 resonators, have relatively pure substrates, which makes them insignificantly affected by gamma radiation and thus immune to it. Another observation has been made regarding our resonators; each device, although identical, reacted differently to the same gamma doses, which could be related to the fact that there are inconsistencies in the fabrication of the same device as mentioned in chapter 5. This enables us to conclude that there cannot be a predicted frequency shift trend for devices, even if they are of the same kind.

Lastly, the neutron irradiation experiment was conducted to test another type of radiation that has not been tested with narrowband, high Q, SAW resonators before. Agreeing with a paper [46] that experimented the effects of neutron radiation on thermosensitive quartz resonators, our resonators experienced random frequency shifts at different dose levels. In addition, they have demonstrated less than 10 ppm frequency shifts for the same dose range, which supports the previously deduced conclusion that these resonators are insensitive to nuclear radiation.

All three experiments show that these resonators are insignificantly affected by gamma and neutron irradiation (if affected at all), even when irradiated up to extremely high level of dose accumulation. The minor changes in frequencies detected seem to have not been due to the effect of radiation on the quartz substrate, where as the effect of slight changes in the environment, which are almost impossible to control even when trying to cancel them out while using the control (standard) devices. These SAW resonators operate at ultra high frequencies, where any movement or slight changes in the environment surrounding the oscillator circuit continuously showed slight changes in the frequency. These slight changes could have easily added up leading to the observed changes and trends in the results.

6.2 Future Work and Recommendations

There are a few recommendations on future work done in this field and/or with these types of devices that I would like to address. If I were to further experiment on SAW resonators, I would attempt the following:

- Coat the surface of device substrates and observe the effect of radiation on devices with various deposited layers;
- test other types of radiation, such as electron and proton radiation;
- vary the dose rate used for each radiation tested; and
- use a remote, wireless, transmitter as part of the oscillator circuit and test the real time effect of radiation on the SAW oscillator.

Papers [43,45] have experimented on SiO_x coated devices and results showed less degradation (smaller frequency shifts) to these device when exposed to nuclear radiation.

Therefore, other materials can be experimented on, where observation of any further stability to the devices may be witnessed. Moreover, these papers, along with others, have tested other types of radiation on SAW resonators or on other quartz resonators. Since it has been proven that the RP1308 resonators are insensitive to gamma and neutron radiation, it is worth studying whether they will also withstand the other types of radiation.

Real-time effect of radiation on these devices, as well as, effects on the oscillator system as a whole is recommended to be examined. This thesis has proven that commercially used resonators, like RP1308 SAW resonators, experience negligible drifts to their oscillation frequencies; however it is vital to study the effect on the oscillator as well. The oscillator circuit, with its electronic components, have a great effect on the oscillation frequency. Also, in the case of neutron irradiation, the resonators were radioactive for some time, which did not allow measurements to be recorded immediately after their irradiation. Online measurements of these devices as they are irradiated or right after irradiation (when radioactive) may show slight different results, especially at much higher irradiation levels, where the radioactivity periods are much longer.

Chapter 7

References

1. J. Scarpulla and A. Yarbrough, "What Could Go Wrong? The Effects of Ionizing Radiation on Space Electronics," The Aerospace Corporation [online]. Available: http://www.aero.org/publications/crosslink/summer2003/03.html

2. B.R. Bhat, N. Upadhyaya, and R. Kulkarni, "Total Radiation Dose at Geostationary Orbit," IEEE Trans. Nucl. Sci., v. 52, pp.530-533, 2005.

3. M. Hoummady, A. Campitelli, and W. Wlodarski, "Acoustic Wave Sensors: Design, Sensing Mechanisms and Applications," Smart Mater. Struct., v. 6, pp. 647-655, 1997.

4. S. Lee, D.D. Stubbs, W.D. Hunt, and P.J. Edmonson, "Vapor Phase Detection of Plastic Explosives Using a SAW Resonator Immunosensor Array," IEEE, pp. 468-471, 2005.

5. X. Chen, M. Cao, Y. Hao, Y. Li, and P. Wang, "A Non-invasive Detection of Lung Cancer Combined Virtual Gas Sensors Array with Imaging Recognition Technique," IEEE, pp. 5873-5876, 2005.

6. C.K. Campell, "Surface Acoustic Wave Devices for Mobile and Wireless Communications," Academic Press, London, UK, 1998.

7. L. Braile, "Seismic Wave Demonstrations and Animations," Purdue University [online]. Available: http://web.ics.purdue.edu/~braile/edumod/waves/WaveDemo.htm

8. J.W. Gardner, V.K. Varadan, and O.O. Awadelkarim, "Microsensors MEMS and Smart Devices," John Wiley & Sons Ltd., 2001.

9. R.P. Buck, E. Lindner, W. Kutner, and G. Inzelt, "Piezoelectric Chemical Sensors," IUPAC Document, Pure and Appl. Chemistry 78, 1139-1160, (2004).

10. J.D. Cheeke, "Fundamentals and Applications of Ultrasonic Waves," CRC Series in Pure and Applied Physics, 2002.

11. SAW_fig1_E.gif [Graphic]. http://www.epsontoyocom.co.jp/english/C_support/aboutFilter/images/SAW_fig1_E.gif

12. Q. Fu, H. Stab, W. Fischer, "Investigation of Single-Finger Interdigital Transducer as Programmable Reflector," IEEE International UFFC Joint 50th Anniv., pp. 2000-2002, 2004.

13. L. Rayleigh, "On waves propagating along the plane surface of an elastic solid," Proceedings of London Mathematical Society, v. 7, pp. 4–11, 1885.

14. L.M. Dorozhkin and I.A. Rozanov, "Acoustic Wave Chemical Sensors for Gases," Journal of Analytical Chemistry, v. 56, pp. 455-474, 2001.

15. E. Berkenpas, S. Bitla, P. Millard, and M. Pereira da Cunha, "LGS Shear Horizontal SAW Devices for Biosensor Applications," IEEE, pp. 661, 2003.

16. F. Josse, and R.W. Cernosek, "Resonant Piezoelectric Devices as Physical and Biochemical Sensors," Marquette University [online]. Available: http://www.ieee-uffc.org/freqcontrol/tutorials/Jose-Cernosek_files

17. U. Wolff, F.L. Dickert, G.K. Fischerauuer, W. Greibl, and C.C.W. Ruppel, "SAW sensors for harsh environments," IEEE Senors Journal v. 1, pp. 410 2001.

18. L. Braile, "Seismic Wave Demonstrations and Animations," Purdue University [online]. Available: http://web.ics.purdue.edu/~braile/edumod/waves/WaveDemo.htm

19. B. Jakoby, and M.J. Vellekoop, "Properties of Love Waves: Applications in Sensors," Smart Material and Structures, v. 6, pp. 668-670, 1997.

20. B. Jakoby, and M.J. Vellekoop, "Design of Love Wave Sensor Devices for the Operation in Liquid Environments," Proc. IEEE Ultrasonic Symposium, pp. 375-379, 1997.

21. J. Ricco, S.J. Martin, T.E. Zipperian, "Surface Acoustic Wave Gas Sensor Based on Film Conductivity Changes," Sensors and Actuators, v. 8, pp. 319, 1985.

22. S. Joshi, "Surface Acoustic Wave (SAW) Flow Sensor," IEEE Trans. UFFC-38, pp. 148-151, 1991.

23. A. Pohl, G. Ostermayer, L. Reindl, and F. Seifert, "Monitoring the Tire Pressure at Cars Using Passive SAW Sensors," IEEE Trans. UFFC, pp. 1-4, 1997.

24. M. Hummady and F. Bastien, "Acoustic Wave Viscometer," Review Science Instrum., v. 62, pp. 1999-2003, 1991.

25. J. Ricco, S.J. Martin, and T.E. Zipperian, "Surface Acoustic Wave Gas Sensor Based on Film conductivity Changes", Sensors and Actuators, v. 8, pp. 319-320, 1985.

26. J. Kondoh and S. Shiokawa, "New Biosensor Using Shear Horizontal Surface Acoustic Wave Device," Jpn. J. Appl. Phys., v. 31, pp. 82-84, 1992.

27. P.A. Banda, W. Wlodarski, and T. Pisarkiewicz, "Theory, design and Operation of a Conductivity Based Surface Acoustic Wave Ozone Sensor," Proc. 8th Inter. Conf. Solid-State Sen. Act., pp. 755-757, 1995.

28. Ballato, "Acoustic Properties of Anisotropic Substrates," IEEE Ultrasonic Sym., pp. 66-68. 2003.

29. T.E. Parker and G.K. Montress, "Precision Surface-Acoustic-Wave (SAW) Oscillators," IEEE Trans. UFFC 35, pp. 342-347, 1988.

30. G.F. Cardinale, J.L. Skinner, and A.A. Talin, "Fabrication of a Surface Acoustic Wave-Based Correlator Using Sep-and-Flash Imprint Lithography," J. Vac. Sci. technology B, v. 22, pp. 3265-3269, 2004.

31. Dr. J. Luxat, notes from EP3DO3-Principles of Nuclear Engineering, McMaster University, 2007.

32. J.R. Lamarsh and A.J. Baratta, "Introduction to Nuclear Engineering," 3rd edition, Prentice Hall, NJ 2001.

33. "What Are the Basic Building Blocks of an Atom?" European Commission [online]. Available: http://ec.europa.eu/research/energy/fi/fi_bs/article_1172_en.htm

34. R.A. Knief, "Nuclear Energy Technology," Hemisphere Publishing Company, Pennsylvania, 1981.

35. EM_Spectrum3_smaill.jpg [Graphic]. http://mynasadata.larc.nasa.gov/images/EM_Spectrum3_small.jpg

36. R.L. Murray, "Introduction to Nuclear Engineering," Prentice-Hall Inc, NY 1954

37. CDE Dosimetry Services [Online]. Available: http://www.internaldosimetry.com/courses/introdosimetry/images/Photelect.jpg

38. Institute of Physics [Online]. Available: http://www.iop.org/activity/education/Teaching_Resources/

39. CDE Dosimetry Services [Online]. Available: http://www.internaldosimetry.com/courses/introdosimetry/image/Annihilation.jpg

40. 1197-6.jpg [Graphic]. http://cph-theory.persiangig.com/1197-6.jpg

41. liquid_drop_E.jpg [Graphic]. http://www2.kutl.kyushu-u.ac.jp/seminar/MicroWorld3_E/3Part3_E/3P33_E/liquid_drop_E.jpg

42. Dr. D. Novog, notes from EP6LO4-Industrial Monitoring and Detection Techniques, McMaster University, 2007.

43. W.J. Stapor, J.H. Hines, D.H. Wilson, "Ionizing Space Radiation Effects on Surface Acoustic Wave Resonators," IEEE Trans. Nuclear Science, v. 38, 1991.

44. G.L. Weaver, M.J. Reinhart, and H.B. Sequeira, "Examination of Detailed Frequency Behavior of Quartz Resonators Under Low Dose Exposures to Proton Radiation," IEEE International UFFC 50th Anniv. Conf., pp. 356-364, 2004.

45. J.H. Hines, and W.J. Stapor "The effects of ionizing radiation on SAW resonators," Ultrasonics Symposium, pp. 471-476, 1990.

46. R. Velcheva, L. Spassov, Y. Filippov, E. Kulagin, and V. Miklayev, "Thermosensitive Quartz Crystal Resonators Under Fast Neutrons and Gamma Rays," Bulgarian Journal of Physics, v. 29, 2003.

47. J.J. Suter, R.H. Maurer, "Low and medium dose radiation sensitivity of quartz crystal resonators with different aluminum impurity content," IEEE Trans. UFFC, v. 34, pp. 667-673, 1987.

48. G.I. Ptakhova, "Effect of Gamma Radiation on the Dielectric Properties of Quarz," Soviet Phy. Journal, pp. 71-73, 1966.

49. RP1308 Data Sheet, RF monolithics, RP1308-110599, 1999.

50. Schematic from Mr. Robert Pasuta, McMaster Nuclear Reactor

51. T.E. Parker, G.K. Montress, "Precision surface-acoustic-wave (SAW) oscillators," IEEE Transactions on UFFC, v. 35, issue: 3, pp. 342-364, 1988.

52. J.R. Srour, C.J. Marshall, and P.W. Marshall, "Review of Displacement Damage Effects in Silicon Devices," IEEE Tran. Nuc. Sc., v. 50, pp. 653-655, 2003

Appendix 1

Results from the first experiment:

Table A1.1: Results of gamma irradiation up to 50 Mrad(Si).

SAW #	*f0 (MHz) before correction**	*f0 (MHz) after correction**	Dose (Mrad(Si))	*f2 (MHz)*	*Δf (MHz)*	*Δf/f0*
1	433.879569	433.880837	0.1667	433.87828	-0.002557	-5.89E-06
2	433.882517	433.883785	5	433.8774	-0.006385	-14.7E-6
3	433.881873	433.881873	5	433.8787	-0.003173	-7.3E-6
4	433.870820	433.87082	5	433.86552	-0.0053	-12.2E-6
5	433.855846	433.855846	10	433.85408	-0.001766	-4.07E-06
6	433.846411	433.846411	10	433.84172	-0.004691	-10.8E-6
7	433.868292	433.868292	15	433.86828	-1.2E-05	-.28E-07
8	433.872280	433.87228	15	433.8723	2E-05	.46E-07
9	433.879869	433.879869	20	433.87812	-0.001749	-4.03E-06
10	433.886010	433.88601	20	433.88262	-0.00339	-7.8E-6
11	433.867860	433.86786	25	433.86572	-0.00214	-4.93E-06
12	433.884723	433.884723	25	433.88246	-0.002263	-5.22E-06
13	433.865812	433.865812	30	433.86498	-0.000832	-1.92E-06
14	433.867992	433.867992	30	433.86624	-0.001752	-4.04E-06
15	433.858362	433.858362	35	433.85928	0.000918	2.12E-06
16	433.876582	433.876582	35	433.87952	0.002938	6.77E-06
17	433.870526	433.870526	40	433.87254	0.002014	4.64E-06
18	433.845454	433.845454	40	433.8464	0.000946	2.18E-06
19	433.890664	433.890664	45	433.88966	-0.001004	-2.31E-06
20	433.865469	433.865469	45	433.86524	-0.000229	-.53E-06
21	433.849315	433.849315	50	433.8464	-0.002915	-6.72E-06
22	433.844745	433.844745	50	433.84822	0.003475	8.01E-06

*** Correction has been made to the frequencies measured according to changes in the frequencies of the controlled devices, in order to cancel out any external effects affecting the performance of the devices.**

Results from the second experiment:

Table A1.2: Gamma irradiation up to 5 Mrad(Si)

SAW#	Dose	*f01 (MHz) before correction*	*f01(MHz) after correction*	*f0R(MHz)*	*Δf01*	*Δf/f01 (ppm)*
1	1	433.869790	433.869350	433.868690	-660.0E+0	-1.521195
2	1	433.875970	433.875530	433.875430	-100.0E+0	-.230481
3	1	433.839350	433.838910	433.837810	-1.10E+3	-2.535503
4	1	433.844050	433.845130	433.844970	-160.0E+0	-0.368795
5	1	433.846650	433.847730	433.848550	820.0E+0	1.890064
1	2	433.869790	433.868450	433.868430	-20.0E+0	-0.0460969
2	2	433.875970	433.874630	433.875150	520.0E+0	1.198503
3	2	433.839350	433.838010	433.836930	-1.080E+3	-2.489408
4	2	433.844050	433.842710	433.842950	240.0E+0	0.553196
5	2	433.846650	433.845310	433.846530	1.220E+3	2.812062
1	3	433.869790	433.868450	433.868630	180.0E+0	0.414872
2	3	433.875970	433.874630	433.875230	600.0E+0	1.382888
3	3	433.839350	433.838010	433.836910	-1.10E+3	-2.535509
4	3	433.844050	433.842710	433.842950	240.0E+0	0.553196
5	3	433.846650	433.845310	433.846650	1.340E+3	3.088658
1	4	433.869790	433.870370	433.870790	420.0E+0	0.968031
2	4	433.875970	433.876690	433.877790	1.10E+3	2.535283
3	4	433.839350	433.839910	433.839270	-640.0E+0	-1.475199
4	4	433.844050	433.844890	433.845470	580.0E+0	1.336883
5	4	433.846650	433.847490	433.849070	1.580E+3	3.641833
1	5	433.869790	433.870310	433.870010	-300.0E+0	-0.691451
2	5	433.875970	433.876470	433.877310	840.0E+0	1.936035
3	5	433.839350	433.839870	433.839330	-540.0E+0	-1.244699
4	5	433.844050	433.844710	433.845150	440.0E+0	1.014188
5	5	433.846650	433.846850	433.848470	1.620E+3	3.734037

Results from the third experiment:

Table A1.3: Neutron irradiation up to 40 sec

SAW #	*f0 (MHz) before correction*	*f0 (MHz) after correction*	time (sec)	*f2 (MHz)*	*Δf (MHz)*	*Δf/f0 (ppm)*
7	433.8539	433.85209	10	433.85603	0.00394	9.08144
8	433.9084	433.90703	10	433.90791	0.00088	2.03
9	433.8728	433.87267	10	433.87223	-0.00044	-1.0
7	433.8539	433.85365	20	433.85695	0.0033	7.6
8	433.9084	433.90807	20	433.91011	0.00204	4.7
9	433.8728	433.87363	20	433.87359	-4E-05	-92.2
7	433.8539	433.85443	30	433.85635	0.00192	4.4
8	433.9084	433.90885	30	433.91207	0.00322	7.4
9	433.8728	433.87341	30	433.87307	-0.00034	-0.7836
7	433.8539	433.85423	40	433.85767	0.00344	7.9
8	433.9084	433.90871	40	433.91041	0.0017	3.9
9	433.8728	433.87369	40	433.87117	-0.00252	-5.8